Title
Spatio-mechanical regulation of Eph receptors at the cell-cell interface

Author
Greene, Adrienne Celeste

Publication Date
2014

Peer reviewed|Thesis/dissertation

Spatio-mechanical regulation of Eph receptors at the cell-cell interface

By

Adrienne Celeste Greene

A dissertation submitted in partial satisfaction of the
requirements for the degree of
Doctor of Philosophy
in
Molecular and Cell Biology
in the
Graduate Division
of the
University of California, Berkeley

Committee in charge:

Professor Jay Groves, Co-chair
Professor David Drubin, Co-chair
Professor Kunxin Luo
Professor David Schaffer

Fall 2014

Spatio-mechanical regulation of Eph receptors at the cell-cell interface

By Adrienne Celeste Greene

Abstract

Spatio-mechanical regulation of Eph receptors at the cell-cell interface

by

Adrienne Celeste Greene

Doctor of Philosophy in Molecular and Cell Biology
University of California, Berkeley

Professor Jay T. Groves, Co-chair
Professor David Drubin, Co-chair

Spatial organization and movement of receptors and ligands at a cell–cell interface is emerging as a key regulatory component of signal transduction. We are particularly interested in understanding the regulation of the EphA2 receptor tyrosine kinase (RTK) movement and spatial reogranization. EphA2 is a unique receptor tyrosine kinase in that it signals in a juxtacrine geometry—EphA2's cognate ligand, ephrinA1, is expressed on the surface of an apposing cell. This unique protein arrangement not only provides a mechanism by which the receptor may experience extracellular forces, but also renders the system challenging to decode. Misregulation of EphA2 often occurs in many aggressive cancers and our lab has recently discovered that EphA2 is sensitive to spatial and mechanical aspects of the cell's microenvironment. We have developed a unique experimental platform in which we use a synthetic supported lipid membrane on a glass substrate to replace the ephrinA1 ligand-expressing cell in a cell–cell contact. This membrane is interfaced with living MDAMB231 breast cancer cells overexpressing EphA2, which effectively mimics a cell-cell junction. The advantage of this approach is the ability to study receptor-ligand interactions using high-resolution microscopy in a live-cell setting as well as modify not only the biochemical content of the membrane, but also the mobility of lipids and proteins. By introducing nanoscale barriers, such as grids patterned on the glass substrate, lipid and protein mobility can be redefined to specific micron-scale features. These diffusion barriers pattern the ligands in the synthetic membrane and allow us to study how spatial organization regulates signaling events. We have developed unique imaging assays to reveal that EphA2 signaling is sensitive to the mechanical properties of a breast cancer cell's microenvironment, which might have direct implications in physical aspects of tumor biology. We have expanded this work to study the structural contributions of Eph receptor clustering at the single molecule level and how this might regulate proper Eph signaling. Finally, we are also probing the cross-talk between membrane-bound ephrinA1 and soluble, secreted ephrinA1 signaling and how EphA2 signaling can be triggered in mechanically-dependent and mechanically-independent mechanisms. Together, these studies provide insight into the regulation of EphA2 signaling and how different aspects of this signaling might be altered in cancer progression.

Table of Contents

List of Figures

Acknowledgements

I would not have made it through graduate school without the love and support of so many different people. During the years of earning my PhD, I have encountered some of the greatest challenges I have ever faced as well as some of the most exciting and wonderful experiences, both in science and in my personal life. Many friends, family, colleagues and mentors have helped get me through those challenges and been part of making those years of earning my PhD so fabulous. I could fill an entire dissertation mentioning everyone who has had such a positive impact on my life, but here I will mention just a few people and hope to express my sincere gratitude for the impact you have had in my life.

- My undergraduate research advisors and mentors – George Bachand, Marlene Bachand, Jerilyn Timlin and Amanda Carroll-Portillo all profoundly influenced my becoming the scientist I am today. They patiently taught me not only how to *do* science, but how to *think* about science. I was given the freedom to creatively explore and learn in an inviting environment where making mistakes was just a part of the learning process. They all contributed deeply to cultivating my excitement about science and learning; I never would have been able to come to Berkeley without the support, mentoring and friendship they each have provided to me and continue to provide to me.
- My thesis committee – David Drubin was a great co-chair; he met with me on several occasions to not only discuss my science, but also my progress and future endeavors and provide advice on what to do next. Kunxin Luo provided excellent insight into the aspects of my project that might have direct implications in the cancer biology fields. I also was fortunate to have two great biophysicists serve on my committee; Jan Liphardt served prior to his move to Stanford and David Schaffer joined my thesis committee afterwards. I have really benefited from their insight, advice and ideas about biophysical misregulation of receptors in cancer.
- My PI – Jay Groves has been a great research advisor and I am so glad I joined his lab. He knows each of his lab members' strengths and weaknesses and has a knack for motivating us to improve those weaknesses, while simultaneously tapping into the strengths each of us provide to the group. He builds a collaborative lab environment, which cultivates strong and lasting working relationships as well as friendships among lab members. I am extremely grateful to have been part of such a unique, strong, fun loving, hardworking and a scientifically impactful lab.
- My research lab – I have such strong and great relationships with all of the Groves lab members. Alex initially recruited me and convinced me to rotate in the lab. Pradeep was my first mentor in the lab and not only convinced me to work on the Eph team, but spent hours teaching me and talking with me about science, even until late into the night. Liz was a great resource of all Eph receptor knowledge and always an initiator of memorable quotes and Groves' lab outings. I cannot thank Mike enough for teaching me so many different techniques, spending countless hours talking about our projects and overall being such a great friend. Sam was an amazing postdoc mentor who really taught me how to critically think about science. We spent hours in the microscope

room and analyzing data and discussing our results and it was that immense amount of time learning from him that really helped me grow as a scientist, of which I am extremely grateful. Finally, I have had great times both scientifically and socially with Meimei, Nicole, Geoff, Rafal, Hector, Chris, Sara, Kate, Jamie, Steven, Monatrice and Jenny. I will always remember the amazing times I have experienced with these extremely talented scientists and amazing friends in the Groves lab.

- My mentors – I want to especially point out that my graduate school mentors have truly helped me through the entire process of graduate school. I have been blessed to have many brilliant and talented scientists provide me with advice, technical training, mentorship and friendship throughout my time here. Sam Lord was one of the most influential mentors I have ever had—thank you! Padmini Rangamani also helped teach me about how to think about my science from a different perspective and has been a great scientific collaborator, as well as a friend. Christa Cortesio and Hector Huang also took lots of time out of their days to provide me with mentorship and advice. Without you all, the path to where I am would have been a lot rougher.
- My undergrad – Jeena came to work in the lab with me right before I took my qualifying exam and was an amazing undergraduate researcher. She learned quickly, efficiently and thoroughly. She very quickly became her own independent research scientist and had her own project in which she was awarded two summer research fellowships. We had a great time working together and I was so proud of her graduation from Berkeley! She was so patient and helped me learn how to be a mentor to student researchers. She has already been very successful and I am excited to continue to watch her amazing progress.
- My graduate school friends – Akemi, Alden, Caitlin, Wendy and Olivia have been there with me through all of the ups and downs of grad school—my qualifying exam, my paper publication, my graduation and so on. Most of my amazing experiences during my time in the program include one or more of these ladies, who have been the best of friends one could ever have.
- My family - Mom, you sacrificed your own time and taught me at home for nine years. I think back to the microscope we had at home to look at our pond water specimens and the heart dissection I did on the kitchen table for mid-school biology (of which you went to great lengths to procure!)—these experiences really helped me learn to love science. You always thought outside of the box and wanted me to receive the best education available and without your patience, time and dedication to my education, I would not be here today—thank you. My study of the biophysical regulation of cancer became even more impactful when you were recently diagnosed with cancer. I hope that my contributions to the field help expand our understanding of disease progression to help women in the same position as you overcome cancer also. Jason, Leslie and Julie—you have been the most fun siblings a sister could ask for. We have always been there for each other and can make each other laugh as nobody else can.
- My oldest of friends - Sara, Ida, Justin and Daniel, you are some of the smartest, funniest and greatest team of friends from my past [and current] days—here's to many more years of friendship through my wild adventures!

Chapter 1: Introduction

Section 1.1: Eph receptor signaling

Eph receptor kinase signaling plays an important role in many cell behaviors[1] including vasculogenesis[2,3], axon guidance[4], and cell migration[5]. The 14 Eph receptors in the human genome constitute the largest family of RTKs[6,7] and all of them signal in a juxtacrine geometry, with the ephrin ligands typically expressed on an apposing cell membrane. The Eph family of RTKs is further divided into two sub-families; the EphA and EphB receptors. EphA receptors preferentially bind to glycosylphosphatidylinositol (GPI)-anchored ephrinA ligands, while EphB receptors preferentially bind to transmembrane ephrinB ligands, while the [8]. This juxtacrine signaling geometry results in a bidirectional signaling motif in which the Eph-expressing cells forward signal into the ephrin-expressing cells and vice versa, rendering the signaling network rather challenging to decode. Eph receptor activation additionally does not seem to follow the canonical RTK dimerization model; rather, Eph activation causes oligomerization resulting not only from Eph–ephrin interactions, but also Eph *cis* interactions mediated through the sushi[9,10] and SAM domains[11] of the Eph receptor. This in turn can propagate ligand-mediated seeding or oligomerization of Eph receptor clusters that is not dependent upon direct ephrin contact[12]. Structural studies confirm that Eph–ephrin clustering is not consistently a direct 1:1 stoichiometry of receptor to ligand binding[9,13]. Additionally, Eph signaling is further complicated by the ability of the receptor to signal in both a ligand-dependent and ligand-independent manner[14]. Together, misregulation of these unique features of both Eph signaling and clustering likely play a role in disrupting the fine-tuning and balance of appropriate Eph receptor signaling in disease progression[15].

Section 1.2: Misregulation of Eph receptor signaling

Misregulation of Eph signaling is linked to a variety of cancers[16,17], with 60–80% of aggressive breast cancers overexpressing EphA2[18–23]. The mechanisms by which EphA2 signaling becomes misregulated are not well understood, due in part to its paradoxical roles: EphA2 has been shown to both promote and suppress tumor progression[21,24]. For instance, simply overexpressing a nonmutated version of EphA2 is sufficient to induce tumorigenesis and metastasis in nontransformed mammary epithelial cells[18], and has been associated with poor patient prognosis[23]. Conversely, activation of EphA2 by ephrinA1 attenuates downstream signaling, as measured by phosphorylated levels of Erk[20] and cell migration[14]. Specifically,

EphA2 is in balance between ligand-dependent and ligand-independent activation[15], and modulating one of these pathways can significantly alter the overall cellular response. There is also a growing recognition that many aspects of receptor signal transduction are context dependent[25,26], and some of the enigmas in EphA2 signaling are likely a result of different cellular microenvironments.

Section 1.3: Mechanical regulation of signaling pathways

Mechanical interactions between cells and their microenvironment are generally thought to be mediated through adhesion molecules such as integrins, with the extracellular matrix, and cadherins, with other cells. However, mechanical influences on signaling are not just restricted to adhesion processes. Spatial organization at the micron-scale coupled with mechanical forces applied to EphA2 have recently been found to alter proximal membrane signaling events. Additionally, the degree and strength of EphA2–ephrinA1 clustering varies systematically across a library of cancer cell lines in correlation with severity of the disease; breast cancers cell lines exhibiting the higest invastion potential seem to have the most tightly clustered EphA2 receptors[27–29]. Thus, physically manipulating EphA2 alters its signaling properties and the physical association between EphA2 receptors differs markedly between diseased and healthy cells. Precisely how physical forces and spatial assembly of the EphA2 receptor leads to altered signaling activity, particularly when related to the state of disease progression is not well understood.

Section 1.4: Endocytosis is a form of signal regulation

Endocytosis is an adhesion-independent internalization mechanism that is regulated mechanochemically and can in turn also regulate RTK signaling[30–34]. Specifically, endocytosis is a regulatory mechanism that controls the persistence of a cellular signal either by 1) physically removing receptors from the cell surface and trafficking those receptors for degradation resulting in signal termination or 2) by physically removing receptors from the cell surface and recycling the receptors back to the membrane for resensitization to the signal resulting in sustained signaling. Internalized receptor–ligand complexes that continue signaling from endosomes can even result in an amplified signal transduction[35]. Misregulated endocytic trafficking has even been implicated in cancer and is an attractive target for therapy[33]. Eph signal activation triggers ligand cleavage and shedding from the apposing cell, which results in deadhesion and repulsion, and ultimately receptor internalization[36,37]. Several molecular details of Eph endocytosis have been discovered[38–40], although the precise mechanism and regulation of Eph endocytosis is not well understood. Modulating endocytosis could directly alter the balance between ligand-dependent and ligand-independent EphA2 signaling in cancer cells[14].

Section 1.5: In vitro reconstitution of the cell-cell junction

Traditionally, Eph-expressing cells have been co-cultured with ephrin-expressing cells to study Eph-forward signaling[37]. However, the juxtacrine EphA2–ephrinA1 signaling geometry is

challenging to study in a simplified environment using high resolution. To overcome the complexity of using co-culture experiments, Eph-expressing cells are cultured as mono-cultures and purified ephrin is presented to the cells in solution, either as a preclustered dimeric version or as a monomeric version. However, while ephrinA1 is known to be secreted and able to activate in certain cellular contexts[16,41–43], we are interested in understanding forward EphA2 signal activation from membrane-bound, monomeric ephrinA1. To study the EphA2–ephrinA1 cell–cell contact and how juxtacrine signaling is regulated by receptor–ligand movement and micron-scale clustering from membrane-bound ephrinA1, we have developed a hybrid system that allows for probing this process using high-resolution microscopy. To do this, the ephrinA1-expressing cell is replaced with a supported lipid membrane displaying monomeric, purified ephrinA1 ligands (Figure 1.1 *A*). A key feature of the supported membrane is its lateral fluidity[44,45], which allows the ephrinA1 ligands to diffuse freely in two dimensions. EphA2-expressing cells can then be seeded onto the ephrinA1-displaying membrane, effectively mimicking a cell-cell contact. This allows for cells to coalesce EphA2–ephrinA1 into large-scale cell–membrane contact regions enriched in EphA2–ephrinA1. Using this experimental platform removes the complexity of the bi-directional signaling and allows EphA2 forward signaling triggered by membrane-bound ephrinA1 to be exclusively studied with high-resolution fluorescence microscopy. We can also take advantage of the adaptability of this platform; we can probe not only the simplified signaling of only membrane-bound ephrinA1, but also more complex situations of both ephrinA1 paracrine and juxtacrine signaling by using different fluorescent labels on the soluble versus the membrane-bound ephrinA1 ligands.

Section 1.6: Spatially and mechanically controlling receptor-ligand reorganization

Our previous work showed that displaying ephrinA1 on a supported lipid membrane resulted in large, micron-scale reassembly of EphA2–ephrinA1 clusters, indicating that oligomerization might be an important regulatory mechanism oh EphA2–ephrinA1 signaling. To directly test this hypothesis, we altered the micron-scale reorganization of receptors and ligands by using electron-beam lithographically to fabricate nano-patterns onto the underlying glass substrate. These patterns were used to restrict the micro-scale diffusion or transport of lipids and the proteins in the supported membrane, while maintaining free lateral mobility within such "corrals"[46] (Figure 1.1 *B*). In turn, EphA2 receptors on the surface of a live cell are subjected to these same physical constraints when they interact with cognate ephrinA1 ligands in the corralled supported membrane[27,28,47,48]. We showed that using this fabrication technique results in confinement of ephrinA1 clusters as shown by Figure 1.1 *C*. This figure depicts the cell–membrane contact area of MDAMB231 breast cancer cells bound to ephrinA1-containing supported membranes on glass substrates patterned with differently sized corrals (1, 3, 5, and 10 μm).

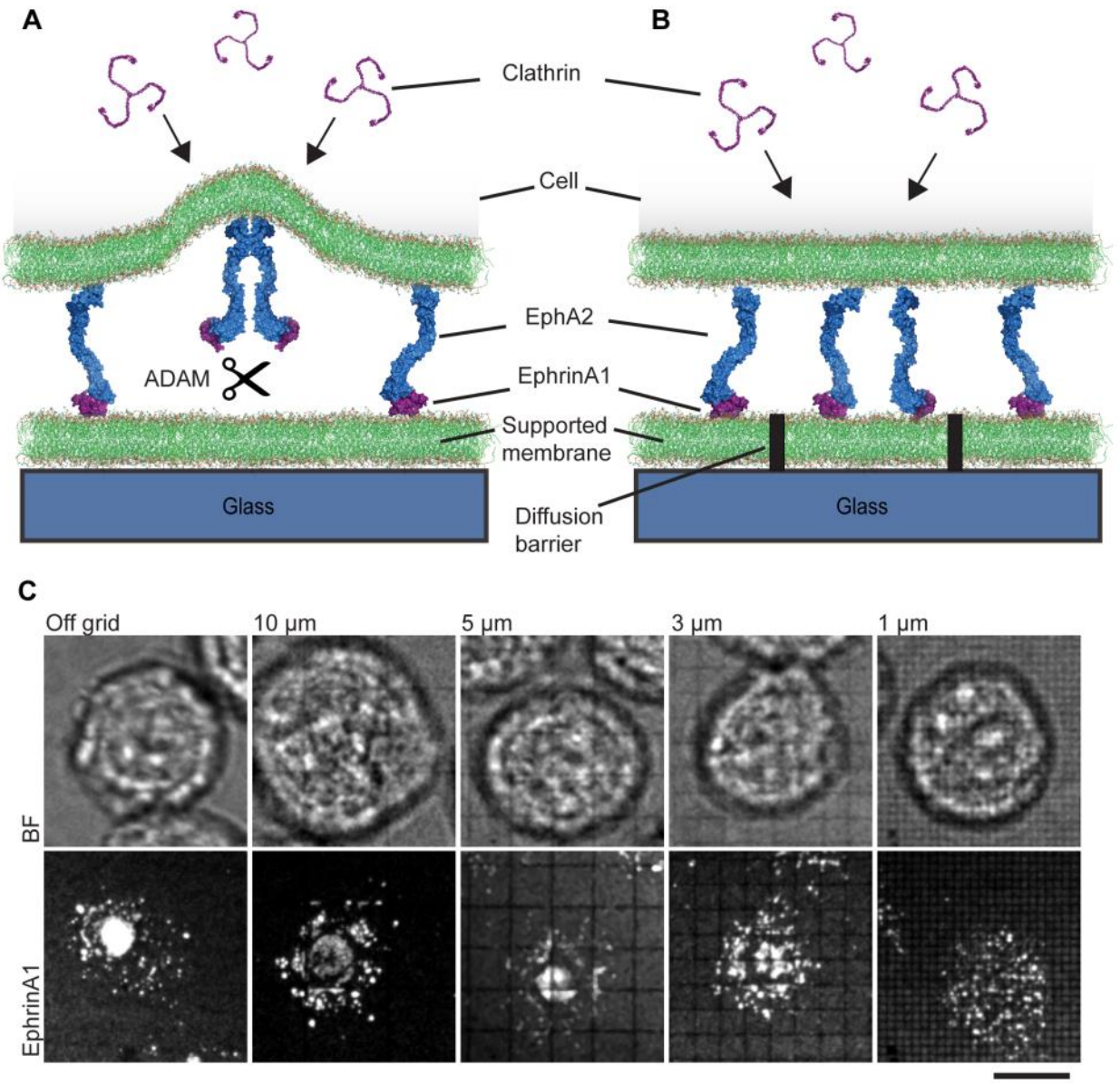

Figure 1.1 Schematic of a cell expressing EphA2 interacting with a supported membrane displaying ephrinA1. A) When on a fluid membrane cells coalesce ephrinA1 into large regions of high concentration and recruit endocytosis molecules. B) When membrane-cell contact sites are physically perturbed using chromium diffusion barriers, endocytosis is altered. C) Bright-field and TIRF images of ephrinA1 at the interface between the cell and supported membrane on an unrestrained substrate and on 10, 5, 3 and 1 µm gridded substrates. Scale bar is 10 µm.

Section 1.7: EphA2 is regulated in a spatio-mechanical manner

Using this reconstituted juxtacrine signaling platform, we recently reported that ephrinA1 ligands bound to a supported membrane are able to trigger EphA2 receptors in living cells as measured by receptor phosphorylation and degradation [28]. Furthermore, we found that EphA2

signaling responds to the spatial and mechanical properties of the cell's microenvironment [27,29]. EphA2–ephrinA1 complexes undergo large-scale actomyosin-driven reorganization at the cell–supported membrane interface, and physical interference with this movement led to distinct changes in downstream signaling and cellular behavior. In particular, we revealed that frustrating EphA2–ephrinA1 micro-scale lateral movement resulted in a significant decrease in the recruitment of a disintegrin and metalloprotease 10 (ADAM10)[27]. ADAM10 has previously been shown to be important in trans-cleavage of ephrins upon Eph binding [49,50], suggesting that ADAM10 activity might be required for the downregulation of Eph signaling. However, the mechanisms by which the mechanical features of the cellular surroundings are translated into these chemical changes, and how this in turn alters downstream EphA2 signaling, remain obscure.

Section 1.8: Conclusions and Motivation

Studying how both space and mechanics, and the coupling of these two mechanisms, regulate EphA2 receptor signaling is key to understanding how Eph receptor signaling is misregulated in disease progression, particularly in cancer metastasis. We have just begun to understand that the EphA2 receptor is unique not only in its non-canonical signaling geometry, but also in its nanoscale and micron-scale oligomerization. All of these unique features likely play a role in regulating the fine-tune balance of ligand-mediated and ligand-independent receptor signaling. When altered by any contributing factor, these balances can be shifted towards misregulation of Eph receptor signaling, which can likely contributes to disease progression of the cell. Understanding in fine detail, both at the nanoscale and micron-scale, how EphA2 receptor signaling is regulated spatio-mechanically will provide great insight into how diseased cell expressing this receptor can be targeted effectively.

Chapter 2

Section 2.1: Introduction

Reconstituting the juxtacrine EphA2–ephrinA1 signaling geometry for use in high-resolution microscopy studies requires replacing the ephrinA1-expressing cell with a supported lipid membrane displaying purified ephrinA1 ligand. Previously, a monomeric version of ephrinA1 was expressed with a C-terminal fusion of the yellow fluorescent protein (ephrinA1-YFP), allowing for direct detection of the ligand upon receptor-binding[28]. While useful for studying membrane-proximal signaling events, we are interested in probing the effects of the spatio-mechanical EphA2 signaling on far-downstream signaling events, including endocytosis. The coding region for ephrinA1 contains a putative ADAM10 cleavage domain located in between the coding sequence for ephrinA1 and the coding sequence for YFP[50,51]. Upon cleavage from ADAM10, the YFP fluorescent tag would likely remain on the supported lipid membrane and unlabeled ephrinA1 would be released from the membrane and perhaps internalized, making it impossible to detect ephrinA1 signaling beyond the supported membrane.

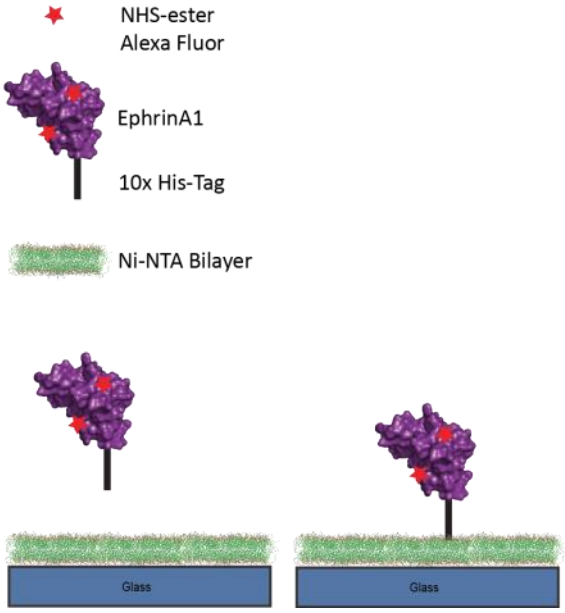

Figure 2.1 EphrinA1-H10 supported membrane assembly. EphrinA1 with a decahistidine tag is purified and organically labelled with an Alexa Fluor dye. Ni-NTA supported membranes are assembled onto solid glass substrates and upon addition of ephrinA1-H10, the protein will be bound to the Ni-NTA lipids via chelation. This creates a laterally mobile ephrinA1-displaying interface.

To overcome this technical difficultly, we designed a non-fluorescent version of ephrinA1 fused to a C-terminal decahistidine tag (ephrinA1-H10), allowing for attachment to lipids with a nickel-chelating nitrilotriacetic acid (NTA) head group (Figure 2.1). We expressed ephrinA1-H10 using a baculovirus expression system to produce a much higher yield of ephrinA1 protein containing the endogenous post-translational modifications (up to 10 mg of protein).

The ephrinA1-H10 construct results in a stable, non-covalent attachment of ephrinA1 to the supported membrane. To visualize the ligand

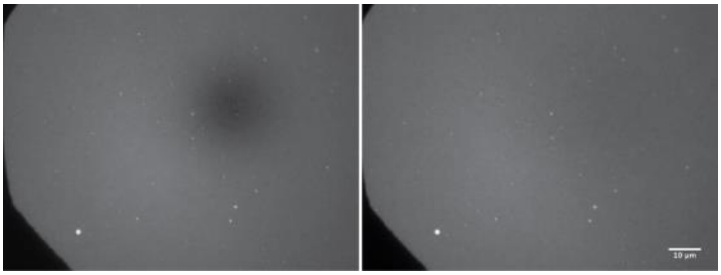

Figure 2.2 Fluorescence recovery after photobleaching of ephrinA1-H10-488. Supported membranes displaying ephrinA1-H10 labelled with Alexa Fluor 488 were assembled. Fluidity of the lipids and proteins was determined using photobleaching. The first image shows the bleached region immediately following bleaching. After one minute another image was taken showing full recovery of the fluorescence indicating that the lipids and proteins were fluid. Scale bar is 10 µm.

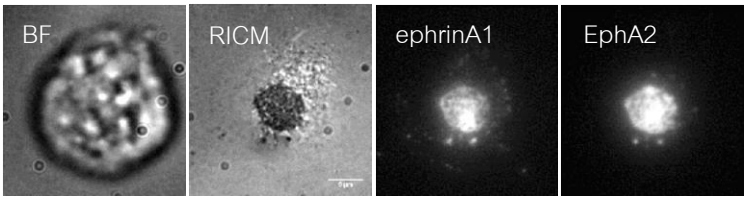

Figure 2.3 Immunofluorescence image of a single MDAMB231 cell interacting with an ephrinA1-H10-647 displaying supported membrane. The first column is a bright field image displaying the outline of the cell. The second column is a reflection interference contract microscopy (RICM) showing the region of the cell that is most closely adhered to the cell membrane. The next two columns are the corresponding fluorescence images of ephrinA1 on the supported membrane which corresponds to EphA2 receptors inside of the cell. Scale bar is 5 µm.

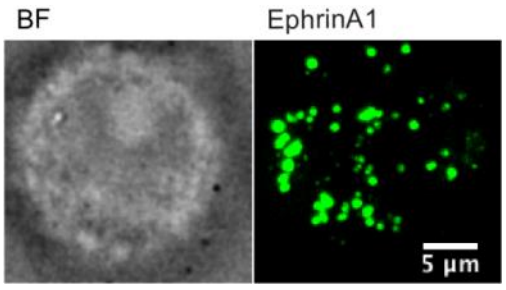

Figure 2.4 Soluble ephrinA1 activates EphA2. Soluble ephrinA1 was detected inside of MDAMB231 cells after 45 min incubation. Here is a single cell image with the bright field image on the left and the projected maximum intensity of internal fluorescent ephrinA1 from a 3D stack on the right.

on the supported membrane, ephrinA1-H10 was organically labeled with NHS-ester Alexa Fluor antibody labeling kits, resulting in non-specific fluorescent labeling of the protein. Upon attachment to the supported membrane, the lateral fluidity of the lipids and thus the adhered proteins can be measured using fluorescence recovery after photobleaching (FRAP) (Figure 2.2). We also confirmed that membranes displaying ephrinA1-H10 are able to activate MDAMB231 cells upon engagement with the bilayer by using immunofluorescence to show colocalization of EphA2 with ephrinA1-H10 (Figure 2.3). Finally, addition of ephrinA1-H10 to cells in solution results in internalization of the ligand further confirming that ephrinA1-H10 is able to activate EphA2 receptors in living cells (Figure 2.4)

While proteins are stable for hours at a time in specific buffers[52], we found that the addition of fetal bovine serum (FBS) in traditional cell culture medium results in the detachment of ephrinA1 from the membrane much more quickly than ephrinA1 in a simple phosphate buffered saline solution (data not shown). The limitations of using ephrinA1-H10 prompted us to design a covalent attachment of ephrinA1 to the supported membrane with a method to site-specifically label the protein. This new attachment allows for long-term visualizations of cells in culture medium containing FBS in addition to single molecule studies of the ligand using a single site-specific fluorescent label. The design is as follows: the C-terminus of the ephrinA1 sequence encodes a biotin-carboxyl carrier protein (or Avi tag) followed by a TEV protease site and a

decahistidine tag used strictly for purification purposes (ephrinA1-BCCP-TEV-H10) Figure 2.5). This protein was expressed using a baculovirus expression system to produce a much higher yield of ephrinA1 protein containing the endogenous post-translational modifications. Following purification using a Ni^{2+}-NTA affinity column to bind to the histidine tag, the protein can be cleaved with TEV protease (see Methods). Cleavage of the histidine tag results in an ephrinA1 fused to BCCP (ephrinA1-BCCP).

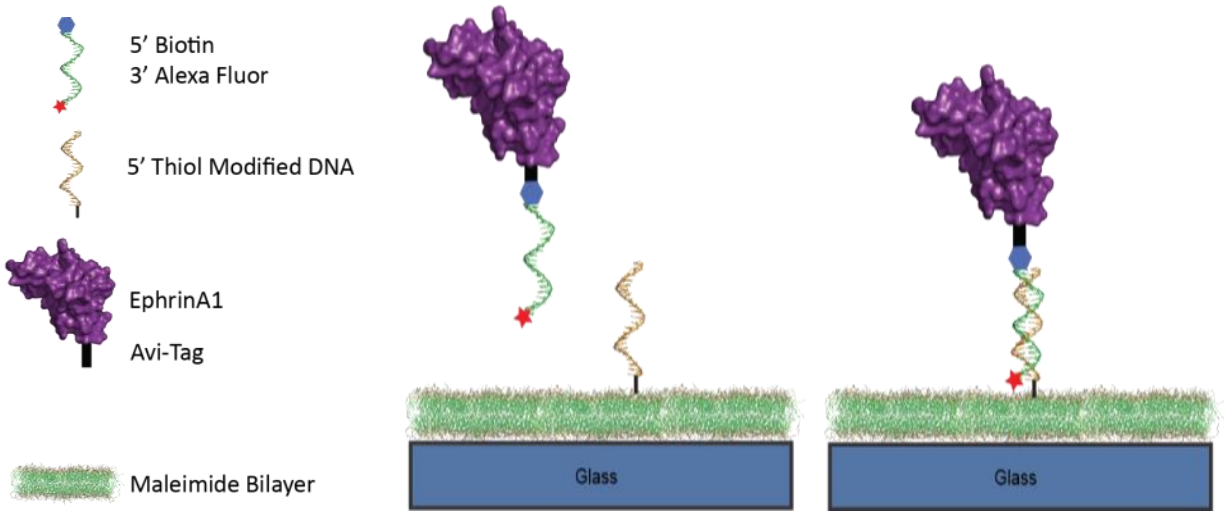

Figure 2.5 ephrinA1-BCCP-TEV-H10 supported membrane assembly. ephrinA1 with a BCCP, TEV and decahistidine tag is purified and attached to a single strand DNA oligo modified with a 5' biotin and 3' Alexa Fluor. Maleimide supported membranes are assembled onto solid glass substrates and upon addition of the complimentary DNA oligo modified with a thiol, the DNA oligo will be bound to the lipids thiol-maleimide chemistry. Addition of the DNA-modified ephrinA1-BCCP allows hybridization and attachment of the protein to the supported membrane creatign a laterally mobile ephrinA1-displaying interface.

EphrinA1-BCCP will selectively bind to a single biotin using the BirA enzyme in an *in vitro* reaction. We used a previously designed 20 base pair single strand DNA oligo sequence and modified it with a 5' biotin to attach directly to ephrinA1-BCCP and a 3' Alexa Fluor 647 for visualization purposes (sequences shown below)[53]. The complementary strand was modified only at the 5' end with a thiol reactive group. A supported lipid membrane containing maleimide lipids will react selectively with the thiol-modified DNA oligo. Following attachment of a single complementary DNA oligo strand to ephrinA1 via the biotin-Avi tag interaction, ephrinA1-BCCP-DNA will attach to the DNA-modified bilayer via DNA hybridization (Figure 2.5).

Single Strand DNA to Attach to the Bilayer (5'→3'):
Thiol—TCATACGACTCACTCTAGGG

Single Strand DNA to Attach to ephrinA1 (5'→3'):
Biotin—CCCTAGAGTGAGTCGTATGA—Alexa Fluor

DNA hybridization provides a near-covalent attachment to the bilayer and a site-specific ephrinA1 label without the use of labelling kits or fluorescent proteins, maintaining ephrinA1 near its endogenous size.

It has also been discovered that soluble ephrinA1 is able to activate EphA2 receptors, in addition to membrane-bound ephrinA1[41,42]. While we are primarily interested in membrane-bound ephrinA1 forward signalling, we confirmed activity of our different ephrinA1 constructs (ephrinA1-YFP, ephrinA1-H10, ephrinA1-BCCP-TEV-H10) in solution using both immunofluorescence and EphA2 degradation assays. The ephrinA1-YFP fusion protein was found to be inactive compared to a commercially-available predimerized ephrinA1 protein and our non-fluorescent fusion protein constructs. These results prompted our exclusive use of the non-fusion protein versions of ephrinA1 for the remainder of our studies.

Section 2.2: Materials and methods

Section 2.2.1: Protein expression and purification

A.

ATGGAGTTCCTCTGGGCCCCTCTCTTGGGTCTGTGCTGCAGTCTGGCCGCTGCTGATCGCCACACCGTCTTCTGGAACAGTTCAAA
TCCCAAGTTCCGGAATGAGGACTACACCATACATGTGCAGCTGAATGACTACGTGGACATCATCTGTCCGCACTATGAAGATCAC
TCTGTGGCAGACGCTGCCATGGAGCAGTACATACTGTACCTGGTGGAGCATGAGGAGTACCAGCTGTGCCAGCCCCAGTCCAAGG
ACCAAGTCCGCTGGCAGTGCAACCGGCCCAGTGCCAAGCATGGCCCGGAGAAGCTGTCTGAGAAGTTCCAGCGCTTCACACCTTT
CACCCTGGGCAAGGAGTTCAAAGAAGGACACAGCTACTACTACATCTCCAAACCCATCCACCAGCATGAAGACCGCTGCTTGAGG
TTGAAGGTGACTGTCAGTGGCAAAATCACTCACAGTCCTCAGGCCCATGTCAATCCACAGGAGAAGAGACTTGCAGCAGATGACC
CAGGATCCACTAGTCTGTACAAGTCCGGACTCAGATCTGGCGGACACCACCACCATCATCATCATCACCACCACTAG

B.

ATGGAGTTCCTCTGGGCCCCTCTCTTGGGTCTGTGCTGCAGTCTGGCCGCTGCTGATCGCCACACCGTCTTCTGGAACAGTTCAAA
TCCCAAGTTCCGGAATGAGGACTACACCATACATGTGCAGCTGAATGACTACGTGGACATCATCTGTCCGCACTATGAAGATCAC
TCTGTGGCAGACGCTGCCATGGAGCAGTACATACTGTACCTGGTGGAGCATGAGGAGTACCAGCTGTGCCAGCCCCAGTCCAAGG
ACCAAGTCCGCTGGCAGTGCAACCGGCCCAGTGCCAAGCATGGCCCGGAGAAGCTGTCTGAGAAGTTCCAGCGCTTCACACCTTT
CACCCTGGGCAAGGAGTTCAAAGAAGGACACAGCTACTACTACATCTCCAAACCCATCCACCAGCATGAAGACCGCTGCTTGAGG
TTGAAGGTGACTGTCAGTGGCAAAATCACTCACAGTCCTCAGGCCCATGTCAATCCACAGGAGAAGAGACTTGCAGCAGATGACC
CAGGCGGATCCGGTGGCGGTCTGAACGACATCTTCGAGGCTCAGAAAATCGAATGGCACGAAAGATCTGAAAACCTGTATTTTCA
GGGCCACCACCACCATCATCATCATCACCACCACTAG

Figure 2.6 DNA sequence for the ephrinA1 constructs designed in this work. A) Sequence for ephrinA1-H10 construct. The sequence for ephrinA1 is highlighted in teal, the sequence for the 10x histidine tag highlighted in yellow and the stop codon is highlighted in red. B) Sequence for ephrinA1-BCCP-TEV-H10 construct. The sequence for ephrinA1 is highlighted in teal, the linkers are not highlighted, the sequence for the biotin carboxyl carrier protein is highlighted in purple, the sequence for the TEV protease site is highlighted in blue, the sequence for the 10x histidine tag highlighted in yellow and the stop codon is highlighted in red.

The soluble, monomeric human ephrinA1 (ephrinA1-H10) sequence (gift of Hans-Christian Asheim, Oslo University, Norway) modified with a C-terminal decahistadine tag (gift of Qian Xu) (Figure 2.6 A) was cloned into the pFastBac™1 (Invitrogen, Carlsbad, CA) expression cassette. Likewise, the soluble, monomeric human ephrinA1 sequences modified with a biotin-carboxyl carrier protein sequence followed by a TEV protease site and a C-terminal decahistadine tag

(ephrinA1-H10-BCCP-TEV-H10) (Figure 2.6 *B*) was cloned into the pFastBac™1 (Invitrogen, Carlsbad, CA) expression cassette. Each expression cassette was transformed into DH10Bac™ *Escherichia coli* cells (Invitrogen, Carlsbad, CA) and DNA was purified to obtain recombinant viral DNA bacmid. SF9 cells (gift of Ann Fischer, UC Berkeley, CA) were transfected with the bacmid DNA using Cellfectin II (Invitrogen, Carlsbad, CA) to generate recombinant baculovirus followed by amplification of viral stocks. SF9 cells were grown in serum-free Sf-900 II SFM insect cell medium and four liters of mid-logarithmic growth phase cells were infected with 50 mL of P2 baculovirus. Cells were centrifuged at 6000 x g and the supernatant containing soluble ephrinA1 was purified using a gravity flow column containing Ni^{2+}-NTA agarose (Qiagen, Valencia, CA) (Figure 2.7 *A*).

Section 2.2.2: Protein preparation and labeling

The ephrinA1-H10 construct was covalently labeled with an Alexa Fluor 647 antibody labeling kit (ephrinA1-H10-647) per manufacturer's instructions (Invitrogen, Carlsbad, CA).

The ~2mg of purified ephrinA1-BCCP-TEV-H10 construct was treated with 1mg TEV protease fused to a histidine tag overnight to cleave the histidine tag from the ephrinA1-BCCP. The protein mixture was purified using a cation exchange column to separate the proteins based upon their isoelectric point. Cleavage of the histidine tag was confirmed by visualizing a shift in size using SDS-PAGE (Figure 2.7 *B*).

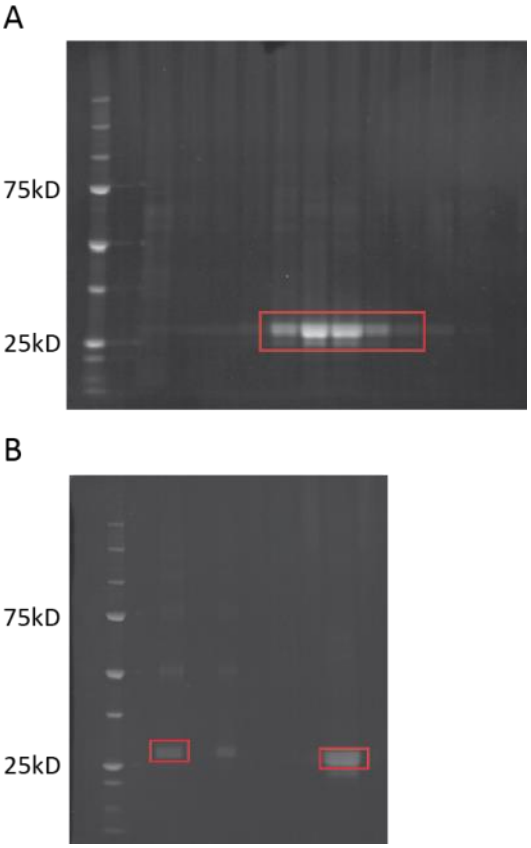

Figure 2.7 SDS PAGE gel of the ephrinA1-BCCP-TEV-H10 protein before and after TEV cleavage. A) Elutions of the purified ephrinA1-BCCP-TEV-H10. Fractions of protein that were collected are boxed in red. B) Size shift in the gel shows that the protein in the last lane runs a slightly faster that the protein in the second lane indicating that the decahistidine tag was successfully cleaved.

Section 2.2.3: Supported membrane assembly

Supported membrane assembly for attachment of ephrinA1-H10

Vesicles composed of 98 mol% 1,2-dioleoyl-*sn*-glycero-3-phosphocholine (DOPC) and 2 mol% of 1,2-dioleoyl-*sn*-glycero-3-[(N-(5-amino-1-carboxypentyl)iminodiacetic acid) succinyl] (nickel salt) (Ni^{2+}-NTA-DOGS) (Avanti Polar Lipids, Alabaster, AL) were made according to standard procedures[54].

Hydrated lipid vesicles were extruded through a 100 nm membrane eleven times, and then a 30 nm polycarbonate membrane three times using an Avanti Mini-Extruder (Avanti Polar Lipids, Alabaster, AL). Supported membranes were then formed on #1.5 Warner brand 25 mm round coverslips according to standard procedures[54]. The supported membrane was then enclosed in an Attofluor cell chamber (Invitrogen, Carlsbad, CA). Membranes were blocked with 1 mg/mL casein solution prior to incubating them with 10 nM ephrinA1-H10 for 1.5 hours according to published methods[52]. Excess protein was thoroughly rinsed away and the membranes were then rinsed with HEPES buffered saline (see below) with 10% fetal bovine serum (Thermo Scientific, Logan, UT) prior to the addition of cells. Other cell media, especially DMEM with 10% fetal bovine serum, contained ingredients that significantly interfered with the nickel chelation of the His-tagged ephrinA1, causing the protein to disconnect from the membrane within minutes at 37°C. In HEPES buffered saline with 10% fetal bovine serum, the His-tagged linkage to the membrane was stable for many hours.

Supported membrane assembly for attachment of ephrinA1-BCCP-TEV-H10

Vesicles composed of 95 mol% 1,2-dioleoyl-*sn*-glycero-3-phosphocholine (DOPC) and 5 mol% of 1,2-dioleoyl-*sn*-glycero-3-phosphoethanolamine-N-[4-(p-maleimidomethyl)cyclohexane-carboxamide](sodium salt) (18:1 PE MCC) (Avanti Polar Lipids, Alabaster, AL) were made according to standard procedures to attach the thiol-modified DNA attached to ephrinA1.

Hydrated lipid vesicles were extruded through a 100 nm membrane eleven times, and then a 30 nm polycarbonate membrane three times using an Avanti Mini-Extruder (Avanti Polar Lipids, Alabaster, AL). Supported membranes were then formed on #1.5 Warner brand 25 mm round coverslips according to standard procedures[54]. The supported membrane was then enclosed in an Attofluor cell chamber (Invitrogen, Carlsbad, CA). Thiol-modified DNA was previously prepared by incubating in 2 mM TCEP and 100 mM HEPES overnight at 4°C to reduce the thiol group, followed by incubation for 1.5 hours at 37°C. DNA was filtered and 1µM DNA was added to the maleimide bilayers for 60-80 minutes. Membranes were rinsed with 30 mL phosphate buffered saline.

Membranes were then incubated with 10 nM ephrinA1-BCCP-DNA for 1.5 hours according to published methods[52]. Excess protein was thoroughly rinsed away and the membranes were then rinsed with HEPES buffered saline (see below) with 10% fetal bovine serum (Thermo Scientific, Logan, UT) prior to the addition of cells.

Section 2.2.4: Image Analysis

Figure 2.4 and 2.5 were created using PDB structures in Pymol and arranged in Adobe Illustrator. The following PDB files were used: ephrinA5 PDB ID: 2X11 [55] and DOPC lipidbook PDB ID: DOPC[56,57].

Section 2.3: Results and discussion

EphrinA1-H10-647 mobility and attachment to the bilayer was confirmed by a fluorescence recovery after photobleaching experiment (Figure 2.2). To confirm that ephrinA1-H10-647 is functional on the membrane, MDAMB231 cells were allowed to adhere to the ephrinA1-displaying membrane. After 45 minutes, cells were fixed and visualized using total internal reflection fluorescence (TIRF) microscopy. EphA2 receptors inside of the cell colocalize with ephrinA1 clusters on the supported membrane, indicating that the membrane-bound ephrinA1-H10 binds to and activates the EphA2 receptors in the cell. Furthermore, we confirmed that ephrinA1-H10 is likewise active in solution by addition of the ligand to MDAMB231 cells. After 45 minutes, ephrinA1 was detected inside of the MDAMB231 cells further corroborating that ephrinA1-H10 is active both in a membrane-bound form and in solution.

EphrinA1-BCCP-TEV-H10 was treated with 1mg of TEV protease to cleave the decahistidine tag. Cleavage of the tag was confirmed by a size shift on an SDS-PAGE gel (Figure 2.7 *B*). The protein was treated with BirA to attach the biotin-modified single stranded DNA to ephrinA1. EphrinA1-BCCP-DNA was purified using a size exclusion column. Functionality of the protein is currently being tested.

These ephrinA1 constructs allow for unique attachments to the supported membrane. EphrinA1 lacking a fluorescent fusion protein provides a way to maintain ephrinA1 in a more-endogenous form while still activating the Eph receptor both in a membrane-bound version as well as in solution. Having a library of ligands with differing attachment chemistries offers versatility in not only how the protein is linked to the membrane, but also to how many proteins can be independently attached. This allows for a hybrid display of different ligands on a supported membrane for use in studying signal crosstalk (e.g. attached integrin ligands as well as EphA2 ligands). These are the ephrinA1 constructs that will be used throughout the remainder of this work.

Chapter 3

Section 3.1: Introduction

Eph receptor signaling plays an important role in many cell behaviors[58] including vasculogenesis[59,60], axon guidance[61], and cell migration[62]. The 16 Eph receptors constitute the largest family of RTKs[63] and all of them signal in a juxtacrine geometry, with the ligands expressed on an apposing cell membrane. EphB receptors preferentially bind to transmembrane ephrinB ligands, while the EphA receptors preferentially bind to glycosylphosphatidylinositol (GPI)-anchored ephrinA ligands[8]. Misregulation of Eph signaling is linked to a variety of cancers[64,65], with 60–80% of aggressive breast cancers overexpressing EphA2[66–71]. The mechanisms by which EphA2 signaling becomes misregulated are not well understood, due in part to its paradoxical roles: EphA2 has been shown to both promote and suppress tumor progression[24,69]. For instance, overexpression of nonmutated EphA2 is sufficient to induce tumorigenesis and metastasis in nontransformed mammary epithelial cells[66], and has been associated with poor patient prognosis[71]. Conversely, activation of EphA2 by ephrinA1 attenuates downstream signaling, as measured by phosphorylated levels of Erk[68] and cell migration[72]. Specifically, EphA2 is in balance between ligand-dependent and ligand-independent activation[72], and modulating one of these pathways can significantly alter the overall cellular response. There is a growing recognition that many aspects of receptor signal transduction are context dependent[73,74], and some of the enigmas in EphA2 signaling are likely a result of different cellular microenvironments.

Mechanical interactions between cells and their microenvironment are generally thought to be mediated through adhesion molecules: integrins, with the extracellular matrix, and cadherins, with other cells. However, mechanical influences on signaling are not restricted to adhesion. Micron-scale spatial organization and mechanical forces applied to EphA2 were found to alter proximal membrane signaling events, and the degree and strength of EphA2–ephrinA1 clustering varies systematically across a library of cancer cell lines in correlation with severity of the disease[75–77]. Thus, physical manipulation of EphA2 alters its signaling properties and the physical association between EphA2 receptors differs markedly between diseased and healthy cells. But precisely how physical forces and spatial assembly of the EphA2 receptor leads to altered signaling activity is not well understood.

Endocytosis is another such adhesion-independent mechanochemically regulated mechanism that in turn can also regulate RTK signaling[78–82], either by physically removing receptors from the cell surface and degrading the proteins (thereby terminating signaling) or by recycling the receptors back to the membrane for sustained signaling. Internalized receptor–ligand complexes that continue signaling from endosomes can even result in an amplified signal[35]. Misregulated endocytic trafficking has been implicated in cancer and is an attractive target for therapy[81]. Eph signal activation triggers ligand cleavage and shedding from the apposing cell, which results in deadhesion and repulsion, and ultimately receptor internalization[83,84]. Several molecular details of Eph endocytosis have been discovered[85–87], although the precise regulation of Eph endocytosis is not well understood. Modulating endocytosis could directly alter the balance between ligand-dependent and ligand-independent EphA2 signaling in cancer cells[72].

To study the cell–cell contact and how juxtacrine signaling is regulated by receptor–ligand movement and large-scale clustering, we have developed a system that interfaces living cells with supported membranes displaying membrane proteins (Figure 1.1 *A*). A key feature of the supported membrane is its lateral fluidity[88,89], which allows the ephrinA1 ligands to diffuse freely in two dimensions and coalesce into large-scale cell–membrane contact regions enriched in EphA2–ephrinA1, effectively mimicking a cell–cell contact. Using this experimental platform removes the complexity of the bi-directional signaling and allows EphA2 forward signaling triggered by membrane-bound ephrinA1 to be exclusively studied with high-resolution fluorescence microscopy. Here we probe the simplified signaling of membrane-bound ephrinA1. Our assay, however, can easily be adapted to study more complex situations of both ephrinA1 paracrine and juxtacrine signaling by using different fluorescent labels on the soluble versus the membrane-bound ligands. The ephrinA1 construct used here lacks a fluorescent fusion protein (unlike the construct used in[76]) and is biologically active in solution (Figure 2.4), corroborating recent studies showing that secreted ephrinA1 is also able to activate EphA2[90–92].

Lithographically fabricated patterns on the underlying glass substrate were used to restrict the micro-scale diffusion or transport of lipids and proteins in the supported membrane, while maintaining free lateral mobility within such "corrals"[93] (Figure 1.1 *B*). In turn, EphA2 receptors on the surface of a live cell are subjected to these same physical constraints when they interact with cognate ephrinA1 ligands in the corralled supported membrane[75,76,94,95]. Figure 1.1 *C* shows the cell–membrane contact area of breast cancer cells bound to ephrinA1-containing supported membranes on glass substrates patterned with differently sized corrals (1, 3, 5, and 10 μm).

Using this reconstituted juxtacrine signaling platform, we recently reported that ephrinA1 ligands bound to a supported membrane are able to trigger EphA2 receptors in living cells as measured by receptor phosphorylation and degradation[28]. Furthermore, we found that EphA2 signaling responds to the spatial and mechanical properties of the cell's microenvironment[27,29]. EphA2–ephrinA1 complexes undergo large-scale actomyosin-driven reorganization at the cell–

supported membrane interface, and physical interference with this movement led to distinct changes in downstream signaling and cellular behavior. In particular, we revealed (20) that frustrating EphA2–ephrinA1 micro-scale lateral movement resulted in a significant decrease in the recruitment of a disintegrin and metalloprotease 10 (ADAM10). ADAM10 has previously been shown to be important in trans-cleavage of ephrins upon Eph binding[49,50], suggesting that ADAM10 activity might be required for the downregulation of Eph signaling. However, the mechanisms by which the mechanical features of the cellular surroundings are translated into these chemical changes, and how this in turn alters downstream EphA2 signaling, remain obscure.

Here, we report that these large regions at the cell–membrane interface that are enriched in EphA2–ephrinA1 recruit proteins involved in endocytosis (namely clathrin, dynamin, and ADAM10) at the exclusion of many other molecules (Figure 3.1). This result prompted us to develop a quantitative single-cell trans-endocytosis assay to probe the effects of EphA2–ephrinA1 reorganization on ligand endocytosis. Using this assay, we found that preventing the large-scale rearrangement and movement of EphA2–ephrinA1 at a cell–cell interface reduces trans-endocytosis of the ligand. Furthermore, we found that the receptor–ligand complex is endocytosed using likely a clathrin mechanism following ligand cleavage from the apposing cell membrane. These results provide mechanistic insight into the spatio-mechanical regulation of EphA2 in breast cancer cells.

Section 3.2: Materials and Methods

Section 3.2.1: Protein expression, purification, and labeling

The soluble, monomeric human ephrinA1 sequence (gift of Hans-Christian Asheim, Oslo University, Norway) modified with a C-terminal decahistadine tag (gift of Qian Xu) was cloned into the pFastBac™1 (Invitrogen, Carlsbad, CA) expression cassette (ephrinA1-H10). The expression cassette was transformed into DH10Bac™ *Escherichia coli* cells (Invitrogen, Carlsbad, CA) and DNA was purified to obtain recombinant viral DNA bacmid. SF9 cells (gift of Ann Fischer, UC Berkeley, CA) were transfected with the bacmid DNA using Cellfectin II (Invitrogen, Carlsbad, CA) to generate recombinant baculovirus followed by amplification of viral stocks. SF9 cells were grown in serum-free Sf-900 II SFM insect cell medium and four liters of mid-logarithmic growth phase cells were infected with 50 mL of P2 baculovirus. Cells were centrifuged at 6000 g and the supernatant containing soluble mEA1-H10 was purified using a gravity flow column containing Ni^{2+}-NTA agarose (Qiagen, Valencia, CA). The mEA1-H10 was then covalently labeled with an Alexa Fluor 647 antibody labeling kit (ephrinA1-647) per manufacturer's instructions (Invitrogen, Carlsbad, CA).

Section 3.2.2: Supported membrane assembly

Vesicles composed of 98 mol% 1,2-dioleoyl-*sn*-glycero-3-phosphocholine (DOPC) and 2 mol% of 1,2-dioleoyl-*sn*-glycero-3-[(N-(5-amino-1-carboxypentyl)iminodiacetic acid) succinyl] (nickel salt) (Ni^{2+}-NTA-DOGS) (Avanti Polar Lipids, Alabaster, AL) were made according to standard procedures[54]. Briefly, hydrated lipid vesicles were extruded through a 100 nm membrane eleven times, and then a 30 nm polycarbonate membrane three times using an Avanti Mini-Extruder (Avanti Polar Lipids, Alabaster, AL). Supported membranes were then formed on #1.5 Warner brand 25 mm round coverslips according to standard procedures[54]. The supported membrane was then enclosed in an Attofluor cell chamber (Invitrogen, Carlsbad, CA). Membranes were blocked with 1 mg/mL casein solution prior to incubating them with 10 nM mEA1-H10 for 1.5 hours according to published methods[52]. Excess protein was thoroughly rinsed away and the membranes were then rinsed with HEPES buffered saline (see below) with 10% fetal bovine serum (Thermo Scientific, Logan, UT) prior to the addition of cells. (Other cell media, especially DMEM with 10% fetal bovine serum contained ingredients that significantly interfered with the nickel chelation of the His-tagged ephrinA1, causing the protein to disconnect from the membrane within minutes at 37°C. In HEPES buffered saline with 10% fetal bovine serum, the His-tagged linkage to the membrane was stable for many hours.)

Section 3.2.3: Grid fabrication

Chromium patterns were fabricated on 25 mm diameter round glass coverslips, which were etched for 5 minutes in piranha solution (3:1 H_2SO_4:H_2O_2), and then spin-coated at 1000 rpm with electron-beam resist (ZEP-520A, Zeon) and conductive polymer (Aquasave, Mitsubishi Rayon). Resist was exposed via electron-beam lithography (CABL9510CC, Crestec). Patterns fabricated included four replicate areas each of 1, 3, 5, 10, and 20 μm grids with line widths of 80 nm. Conductive polymer was removed by rinsing with deionized water, and then resist was developed for 1 minute in isoamyl acetate. Chromium with thickness of 7 nm was deposited by electron-beam evaporation (EB3 e-beam evaporator, Edwards). Resist mask was lifted off by sonicating in methylene chloride for 10 minutes.

Section 3.2.4: Cell culture

MDAMB231 breast-cancer cells (gift of Ann Fischer, UC Berkeley, CA) were cultured in DMEM with Glutamax (Invitrogen, Carlsbad, CA) supplemented with 10% fetal bovine serum (Thermo Scientific, Logan, UT). Cells were stripped from culture flasks using Cellstripper (Mediatech, Manassas, VA) and resuspended in 1x HEPES buffered saline (20 mM HEPES, 137 mM NaCl, 5 mM KCl, 0.7 mM $Na_2HPO_4 \cdot 7H_2O$, 6 mM D-glucose, 1 mM $CaCl_2 \cdot 2H_2O$, 2 mM $MgCl_2 \cdot 6H_2O$) with 10% fetal bovine serum for experiments.

Section 3.2.5: Immunostaining, inhibitor and transferrin experiments

Approximately 300,000 cells were added to each mEA1-647 supported membrane chamber and allowed to engage the membrane for 45 min in a cell culture incubator at 37°C with 5% CO_2.

Chambers were then rinsed with 5 mLs phosphate buffered saline (PBS) followed by cell fixation with ultra-pure 4% paraformaldehyde (Polysciences, Warrington, PA) in 1x PBS for 15 min and finally a 10 mL 1x PBS rinse. For antibody staining, cells were permeabilized with 0.01% Triton X-100 in 1x PBS for 5 min and blocked with 1% bovine serum albumin (BSA) in 1x PBS at 4°C overnight. Mouse monoclonal α-ADAM10 primary antibody (Santa Cruz Biotechnology, Inc., Dallas, TX) was added to the cells at a 1:200 dilution in 1% BSA in 1x PBS for 40 min at room temperature. Chambers were rinsed with 10 mL 1% BSA in 1x PBS and a 1:200 dilution of goat α-mouse secondary antibodies conjugated to Alexa Fluor 488 (Invitrogen, Carlsbad, CA) was added to the chambers for 20 min at room temperature followed by a 10 mL rinse with 1x PBS.

To inhibit the clathrin terminal domain, cells were stripped from culture flasks using Cellstripper (Mediatech, Manassas, VA) and resuspended in 1x tris buffered saline (TBS) with 25 μM Pitstop2 or matching volumes of dimethyl sulphoxide (DMSO) control (Abcam, Cambridge, MA) for 10 min in a cell culture incubator at 37°C with 5% CO_2. To completely remove the inhibitor, cells were centrifuged for 3 min at 500 g, washed with 1x TBS, spun down again and resuspended in 1x HEPES buffered saline with 10% fetal bovine serum prior to adding to the membrane.

To inhibit ADAM10 and ADAM17, 10 μM INCB003619 (Incyte Corp, Wilmington, DE) (or matching volumes of DMSO control) was added to cells in a culture flask for 24 hours. Cells were then stripped from culture flasks using Cellstripper (Mediatech, Manassas, VA) and resuspended in 1x HEPES buffered saline with 10% fetal bovine serum prior to adding to the

Construct	***Vector***	***Fluorescent Protein***	***Source***
Human clathrin light chain	pN1	n-terminal TagRFP-T	Dr. David Drubin, UC Berkeley, CA[96]
Human dynamin2	pN1	n-terminal EGFP	Dr. David Drubin, UC Berkeley, CA[96]
Human caveolin1	pN1	n-terminal RFP	Dr. David Drubin, UC Berkeley, CA
CD52 GPI anchor	pN1	n-terminal EGFP	Dr. Björn Lillemeier and Dr. Mark Davis, Stanford University, CA
KRas anchor	pN1	n-terminal mCherry	Dr. Nick Endres and Dr. John Kuriyan, UC Berkeley, CA
Lck anchor	pN1	c-terminal mCherry	Dr. Hector Huang and Dr. Jay Groves, UC Berkeley, CA[97]
RhoA anchor	pN1	n-terminal mCherry	Dr. Hector Huang and Dr. Jay Groves, UC Berkeley, CA[97]
PLCδ PH domain	pC1	c-terminal GFP	Dr. Tobias Meyer[98] , Addgene plasmid 21179
Mouse cSrc anchor	pN1	c-terminal mCherry	Dr. Hector Huang and Dr. Jay Groves, UC Berkeley, CA, Addgene plasmid 17685
Mouse cSrc protein	pN1	c-terminal mCherry	Dr. Hector Huang and Dr. Jay Groves, UC Berkeley, CA, Addgene plasmid 17685
Human utrophin	pcs2	n-terminal EGFP	Dr. William Bement, University of Wisconsin, WI[99]

membrane.

To monitor transferrin uptake, cells were stripped from culture flasks using Cellstripper (Mediatech, Manassas, VA) and resuspended in 1x HEPES buffered saline with 10% fetal bovine serum and 25 µg/mL transferrin conjugated to Alexa Fluor 568 (Invitrogen, Carlsbad, CA), immediately prior to prior to adding to the membrane.

Section 3.2.6: Transfection reagents

For live-cell imaging experiments, cells were seeded in a 6-well plate, allowed to adhere and rinsed with 1x Dulbecco's PBS prior to changing the cell medium to low-serum Opti-MEM (Invitrogen, Carlsbad, CA). Following manufacturer's instructions, cells were transfected for 5-8 hours using 10 µL Lipofectamine 2000 (Invitrogen, Carlsbad, CA) and 2.5 µg of the following DNA constructs (Table 1):

Section 3.2.7: Spinning disk confocal and total internal reflection fluorescence (TIRF) microscopy

All microscopy hardware was controlled with and images were acquired using Micro-Manager [100]. Microscopy was performed on a motorized inverted microscope (Nikon Eclipse Ti-E/B, Technical Instruments, Burlingame, CA) equipped with a Nikon 100x Apo TIRF 1.49 NA objective lens, motorized Epi/TIRF illuminator, motorized Intensilight mercury lamp, Perfect Focus system, and a motorized stage (ASI MS-2000, Eugene, OR). Lasers included the following: 200 mW 488 nm Ar-ion laser (Spectra Physics 177G, Santa Clara, CA), 100 mW 561 nm optically-pumped solid state laser (Coherent Sapphire, Santa Clara CA), and 100 mW 640 nm diode laser (Coherent Cube, Santa Clara CA). Lasers were controlled using an acousto-optic tunable filter (AOTF) and aligned into a dual-fiber launch custom built by Solamere (Salt Lake City, UT): one single-mode polarization maintaining fiber (Oz Optics, Ottawa, Canada) was connected to a TIRF illuminator, while the other was connected to the spinning disk confocal unit.

A spinning disk confocal head was custom fit to the microscope and camera (Yokogawa CSU-X1-M1N-E, Solamere, Salt Lake City, UT). The dichroic in the spinning disk head was a T405/488/568/647 multiline (Semrock, Rochester, NY). Emission filters were the following from Chroma (Bellows Falls, VT) and in a custom-mounted filter wheel (ASI FW-1000, Eugene, OR): ET525/50M, ET605/52M, and ET700/75M. Confocal images were captured using a 1024×1024 pixel electron-multiplying CCD camera (Andor iXon3 888, Belfast, Ireland), typically at gain setting 200 and with pixels binned 2×2 for higher signal-to-noise. Axial slice step size was 0.5 µm and extended 20 µm above the coverslip.

TIRF, reflection interference contrast microscopy (RICM), and bright field images were collected on an Orca-R2 interline CCD camera (Hamamatsu, Hamamatsu, Japan). Dichroics were 2 mm thick and mounted in metal cubes to preserve optical flatness: ZT488rdc, ZT561rdc, and ZT640rdc. Long-pass emission filters included: ET500lp, ET575lp, and ET660lp. Bandpass

emission filters were located below the dichroic turret in a motorized filter wheel (Sutter Lambda 10-3, Novato CA): ET525/50m, ET600/50m, and ET700/75m. RICM was performed using a 50/50 beamsplitter with a D546/10x filter. All TIRF filters and dichroics were from Chroma (Bellows Falls, VT).

Live-cell imaging was performed using a stage-top incubator and objective heater (Chamlide TC-A, Quorum Technology, Guelph, Canada).

Section 3.2.8: Image analysis

All quantitative image analysis was performed using the ImageJ bundle Fiji [101]. For Figure 3.1, intensity ratios were measured for the transfected molecules with ephrinA1 both in and out of ephrinA1-enriched regions. Based on TIRF and RICM images, ephrinA1-enriched regions and non-ephrinA1 regions were identified. Intensities of the transfected molecules at both regions were measured using Fiji, for each type of molecule and an average of 12 cells were analyzed. In each cell, 3 spots in and out of ephrinA1-enriched regions of each cell were chosen, respectively.

For quantifying ephrinA1 endocytosis, the first few slices of the confocal stacks were removed, thus eliminating the membrane fluorescence and including fluorescence signal only from inside the cell for further analysis. EphrinA1 punctate spots were automatically identified using the Fiji analysis function 3D Objects Counter[102], with a threshold set well above the background (typically three times the average background pixel value) and minimum and maximum spot sizes to eliminate spurious pixels or abnormally large fluorescent blobs (e.g. 5–200 pixels). For several random cells in each sample, mask images outputted from the 3D Objects Counter were visually inspected and compared to the raw data to ensure that the puncta were adequately quantified. For some samples, the raw images were first blurred using a 1 pixel Gaussian filter before further analysis to increase the accuracy of the automatic object identification.

The Pitstop2-treated cells had slightly dimmer membrane slices on average compared to DMSO control cells. To ensure that the change in endocytosis we measured was a result of Pitstop2 treatment and not due to the amount of ephrinA1 available to the cells, we introduced a simple correction factor based on the membrane brightness on a cell–by-cell basis. The correction factor eliminated the already weak correlation between membrane brightness and number of internal ephrinA1 puncta (Figure 3.2), but did not eliminate the significant difference in endocytosis for Pitstop2-treated versus control cells. For grid experiments and cells treated with INCB003619, this correction was not necessary, because we observed no difference in the average brightness of the membrane slices.

For the 3D time lapse of the living cell in Figure 3.4 and the cells on grids in Figure 3.7 *A*, confocal stacks were first blurred using a 1 pixel Gaussian filter, and then the Interactive Stack Rotation plugin in Fiji was used to force the voxels to be cubes (the plugin uses linear interpolation to add extra z slices); the 3D rendering was performed using UCSF Chimera[103]. To normalize the grid plot in Figure 3.7 *C*, the average number of internal ephrinA1 puncta was

rescaled for each sample (which contained multiple repeats of each grid pattern) so that the value on 20 μm grid pitches (or off grid for one sample) was unity, so that each sample would be directly comparable. The actual the average value at 20 μm is 4.05 puncta/cell, so each value in Figure 3.7 *C* was divided by 4.05.

For the radial profile analysis in Figure 3.2, the "Radial Profile Plot" ImageJ plugin written by Paul Baggethun was used. All plots were created and statistical test were run using GraphPad Prism.

Figure 1.1 *A-B* was created using PDB structures in Pymol and arranged in Adobe Illustrator. The following PDB files were used: clathrin triskelion PDB ID: 3IYV [104], EphA2–ephrinA5 PDB ID: 2X11 [55] (note that the structure of the full extracellular domain of EphA2 in complex with ephrinA1 is not available so this structure was used instead) and DOPC lipidbook PDB ID: DOPC[56,57].

Section 3.3: Results

Section 3.3.1: EphA2-ephrinA1 complexes recruit endocytosis molecules

In order to provide insight into the components contributing to the mechanical sensitivity of the EphA2 signaling pathway, we sought to understand the biomolecular composition of the large regions of the cell–membrane interface enriched in EphA2–ephrinA1. To find proteins that colocalize with EphA2–ephrinA1 complexes, we screened through a library of candidate signaling molecules using live-cell transfection of fluorescently-tagged proteins. TIRF microscopy was used to simultaneously visualize ephrinA1 at the cell–supported membrane interface as well as the intracellular signaling molecule. By measuring the fluorescence intensity ratio of the candidate molecule to ephrinA1 both inside and outside the ephrinA1-enriched regions, molecules fell into four distinct spatial categories: molecules either were homogenously distributed throughout the cell membrane, or they colocalized with, anti-localized with, or formed a ring around ephrinA1-enriched regions (Figure 3.1 and 3.3). Interestingly, the only molecules found to be enriched at EphA2–ephrinA1 were the endocytosis components clathrin and dynamin, as well as ADAM10, at the exclusion of many other molecules. Actin formed a ring around the ephrinA1-enriched regions, consistent with our previous results that receptor reorganization is driven by actomyosin contractility[27]. The DiI and the GPI anchor lipid-associated molecules were found to be homogenously distributed across the cell membrane. These localization results indicate that the ephrinA1-enriched regions are sites of clathrin-mediated endocytosis. Therefore we hypothesized that the signaling sensitivity to physical patterning that we previously observed[27] may be related to endocytosis of the RTK and trans-endocytosis of its ligand from the juxtaposed membrane.

Section 3.3.2: Trans-endocytosis assay development

In order to test this hypothesis, we developed a quantitative 3D fluorescence assay to characterize the trans-endocytosis of ephrinA1 bound to EphA2. Fluorescently labeled ephrinA1

was imaged inside of breast cancer cells using spinning disk confocal microscopy. Figure 3.4 shows time-lapse 3D projections of ephrinA1 internalization over 50 minutes, demonstrating ephrinA1 endocytosis increasing over time. Immediately after the single cell landed on the ephrinA1-containing supported membrane, ephrinA1 was enriched in regions of contact between the cell and supported membrane as the cell rounds and EphA2 expressed on the surface of the cell bound ephrinA1; those EphA2–ephrinA1 complexes coalesced into large "clusters" or regions of high EphA2–ephrinA1 concentration. By 30 and 50 minutes, cell–membrane contact sites increased in size and punctate ephrinA1 spots became visible inside of the cell.

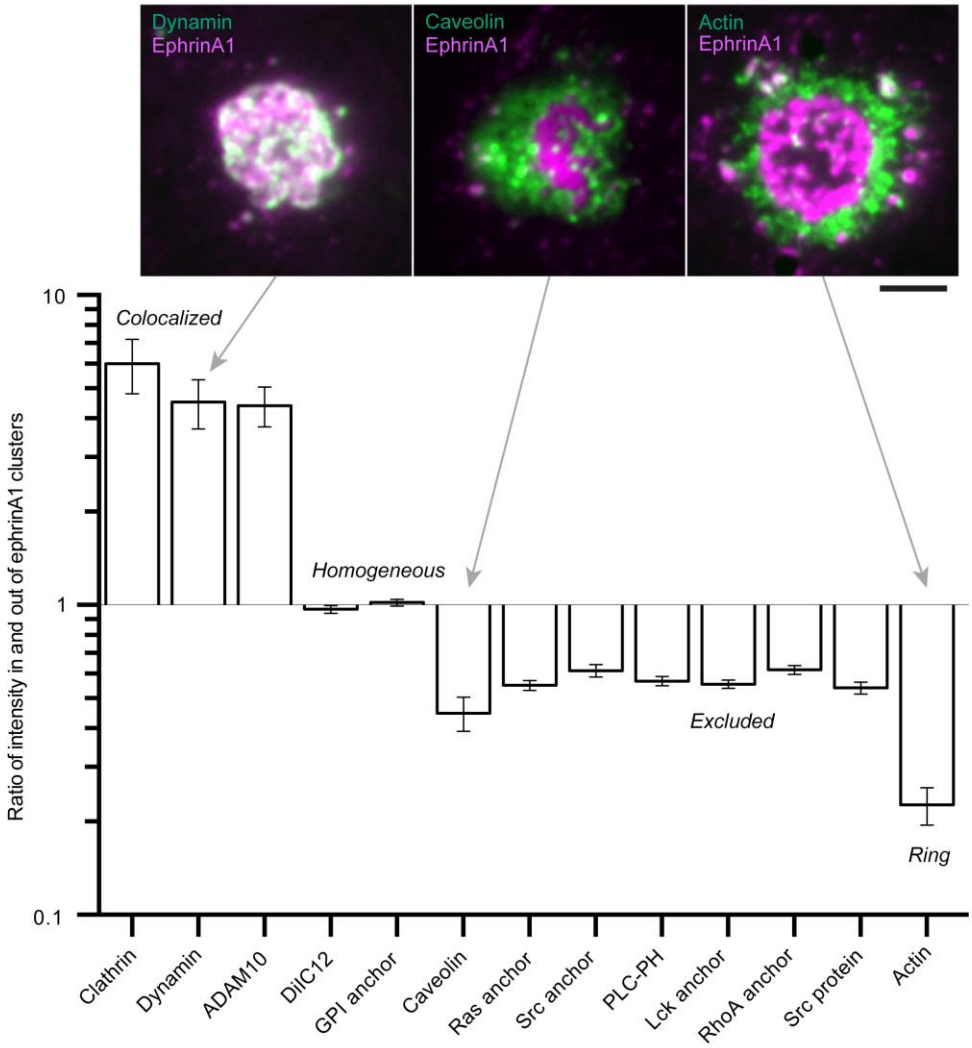

Figure 3.1 Molecular physiology of the EphA2-ephrinA1 contact sites. The ratio of fluorescence intensity within and outside regions of ephrinA1 enrichment is a measure of whether the cellular component is recruit to (values >1) EphA2-ephrinA1 or excluded from (values <1) those sites; values near 1 indicate homogenous distribution throughout the cell membrane. Clathrin and dynamic are colocalized with ephrinA1, caveolin is antilocalized with ephrinA1, and actin forms a ring around the large EphA2-ephrinA1 contact sites. Insets are TIRF microscopy images showing MDAMB231 cells at the membrane-cell interface. The images are false color overlays

Because the only fluorescent molecule in the assay was ephrinA1, the fluorescence signal inside the cell is a direct measure of the amount of ligand trans-endocytosed from the supported membrane. Furthermore, we found that the intensity per ephrinA1 punctate spot is relatively narrowly distributed (Figure 3.6), so we further streamlined the assay by simply counting the number of ephrinA1 puncta per cell as a measure of internalized protein. Counting internal puncta yields similar results to total internal intensity (Figure 3.6), but counting simplifies the analysis greatly, because it is not necessary to subtract background and dark counts; therefore background differences and user-defined thresholds do not influence the results and the counting analysis is more robust. To automate the process, we used simple image-analysis software to identify spots in three dimensions (see Methods). This method provides a simple and reliable assay for detecting single-cell endocytosis, and it eliminates the high variability inherent in antibody staining to quantify internalized signaling molecules.

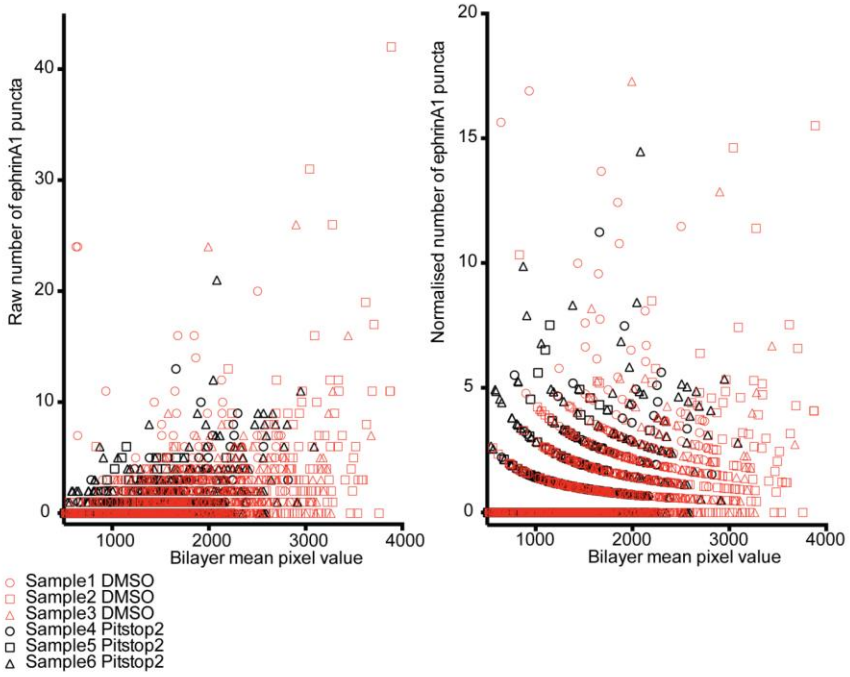

Figure 3.2 Correction for Pitstop2-treated samples to account for different ephrinA1 intensities. (*A*) There exhibited a very weak correlation between the amount of ephrinA1 at the cell-bilayer interface and amount of internalized ephrinA1 for three control DMSO samples (*red*) and three Pitstop2-treated samples (*black*). (*B*) The weak correlation in (*A*) is eliminated by correcting for ephrinA1 brightness at the cell–bilayer interface for the same samples.

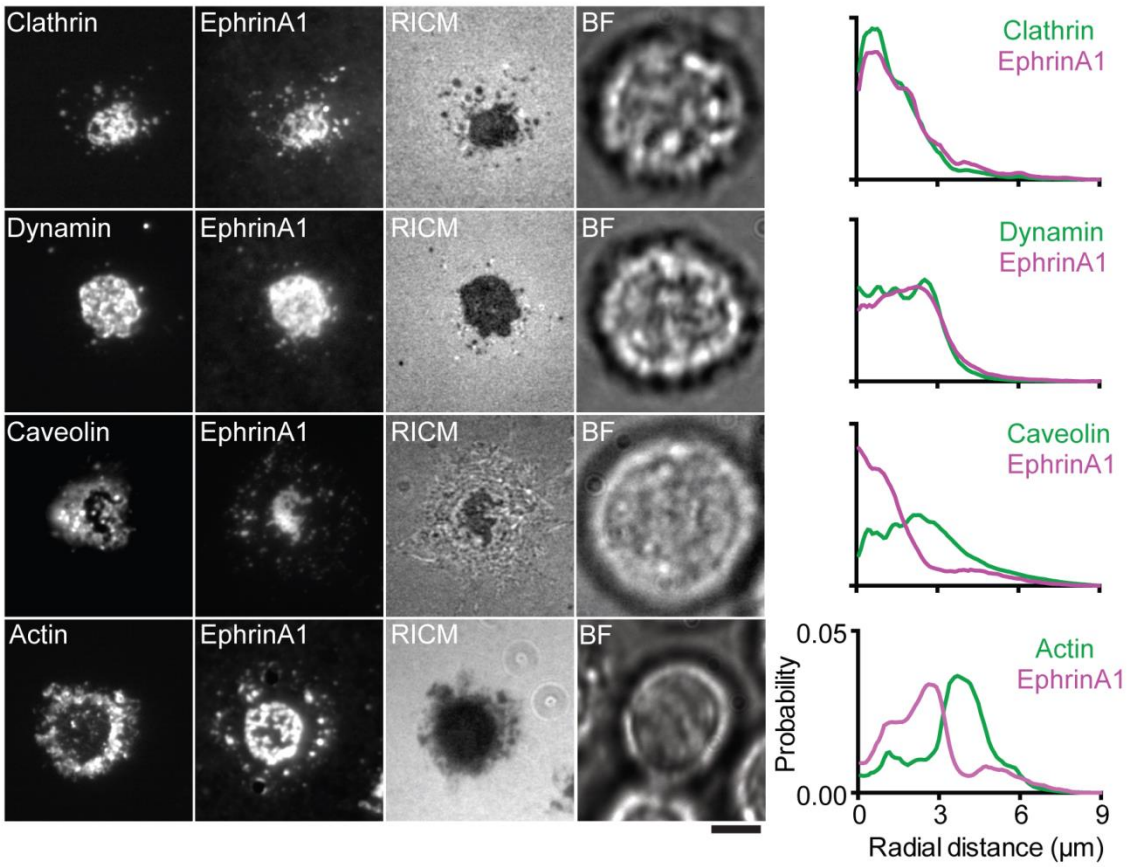

Figure 3.3 TIRF microscopy images showing MDAMB231 cells expressing different fluorescently-tagged molecules. The images in the first column were taken using TIRF microscopy and are representative images of cells expressing the indicated fluorescently-tagged molecules (clathrin, dynamin, caveolin and actin). The images in the second column were also taken using TIRF microscopy and show ephrinA1 (labelled using Alexa Fluor 647) at the membrane-cell interface. The images in the third column were taken using RICM, demonstrating that the ephrinA1-enriched regions are closest contact to the bilayer. The images in the fourth column were taken using bright field microscopy. The radial profile plots (of the specific cells on the left) help clarify that clathrin and dynamin are colocalized with ephrinA1, caveolin is anti-localized with ephrinA1, and actin forms a ring around the large ephrinA1-enriched region. The radial profile plots are normalised so that the area under each curve sums to unity. Scale bar is 10 μm.

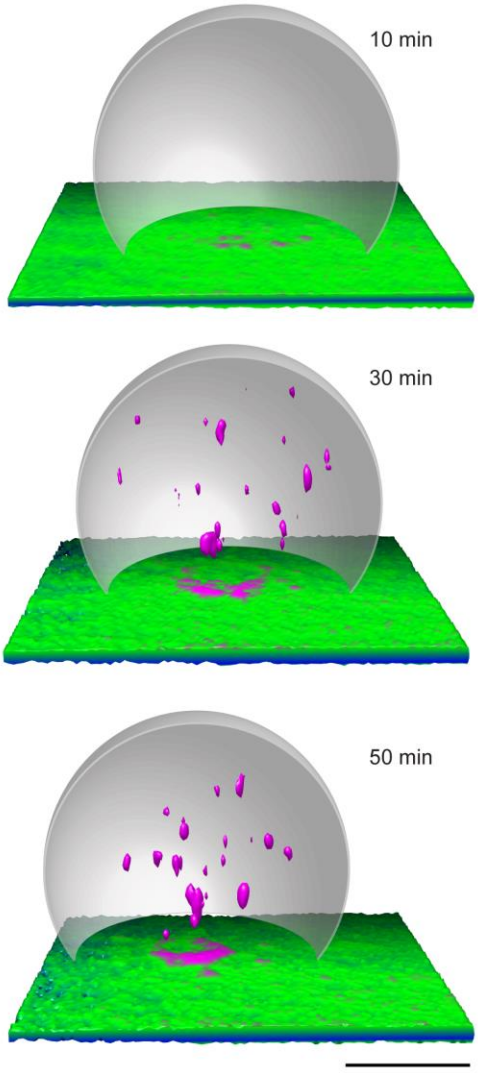

Figure 3.4 Time-lapse 3D reconstructions of confocal stacks of a single living MDAMB231 cell as it lands on an ephrinA1-supported membrane. The cell coalesces EphA2-ephrinA1 into large contact regions at the interface, and then internalizes the receptor and ligand over time. Only ephrinA1 is fluorescently labeled (with Alexa Fluor 647), but the images are pseudocolored to encode height above coverslip (*blue/green* for near the coverslip and *magenta* for > ~1µm above). The gray dome approximates the cell outline. (See Figure 3.5 for a simple grayscale rendering.) Only spots well above the coverslip and membrane-cell interface (typically 3 µm) were included in the analysis. For experiments quantifying endocytosis in hundreds of cells, samples were fixed at 45 min. Scale bar is 10 µm.

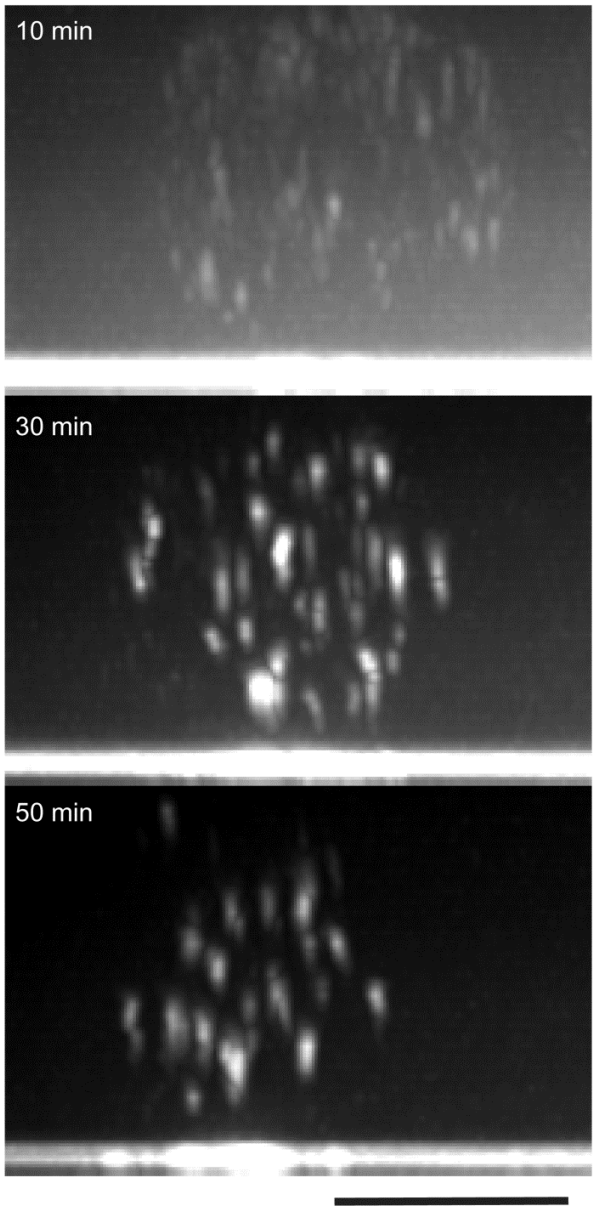

Figure 3.5 A grayscale rendering of cells landing on a supported membrane displaying fluorescent ephrinA1. This is a different rendering of the 3D data than Fig. 3; instead, these images are 2D projections along the *xz* plane. The supported membrane is at the bottom of each frame. Scale bar is 15 µm.

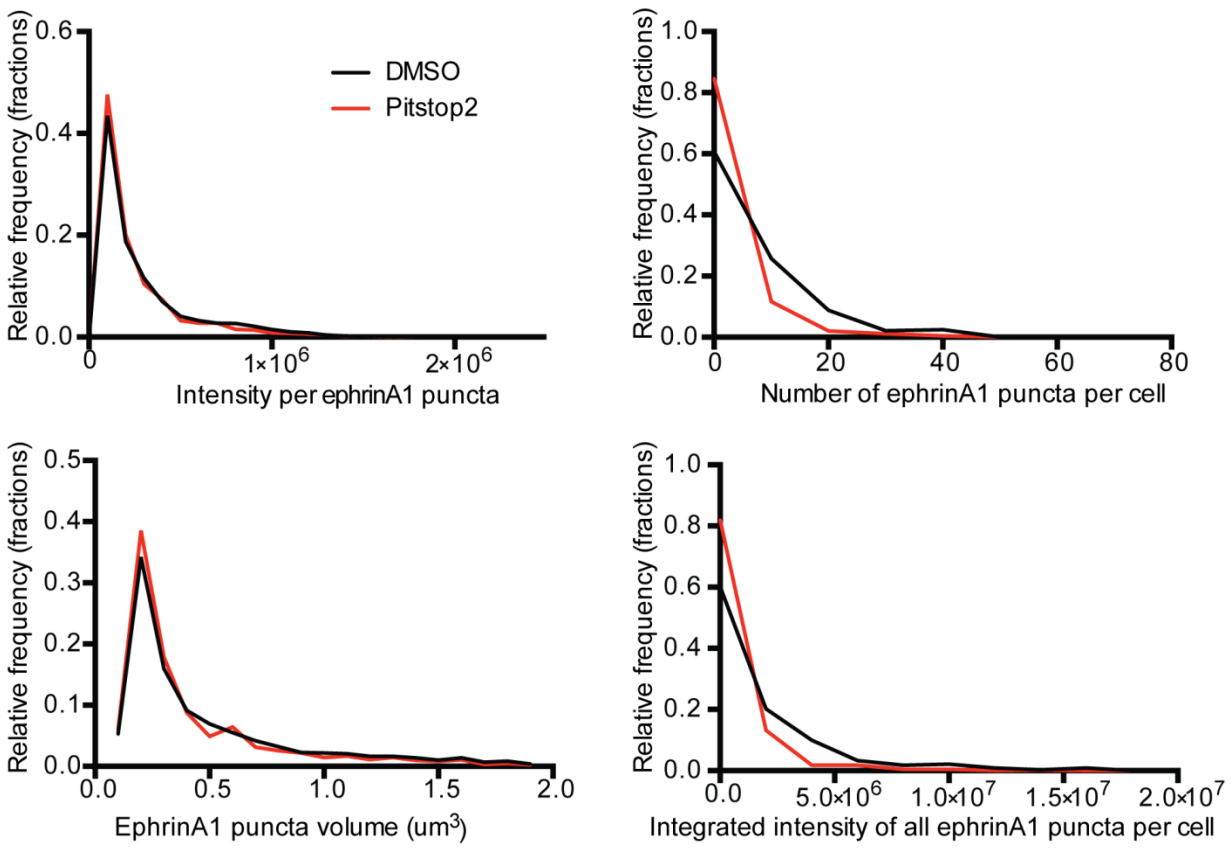

Figure 3.6 Distributions of intensity per puncta, volume per puncta, number of puncta per cell, and total summed intensity of puncta per cell. The intensity and volume per punctate spot is narrowly distributed and identical for different cell treatments. The data is for Pitstop2 drug treatment compared to DMSO treatment, though this trend is also consistent for cells on grid-patterned substrates. The main contribution to changes in total internal cell intensity is changes in number of puncta per cell.

Section 3.3.3: Trans-endocytosis is altered as a function of EphA2-ephrinA1 spatial reorganization

Using this trans-endocytosis assay, we examined if ephrinA1 endocytosis is affected by mechanical properties of the cell–membrane interface. Specifically, we physically hindered EphA2–ephrinA1 reorganization in breast cancer cells that highly overexpress EphA2[27] using patterned supported membranes containing ephrinA1. After incubating on the membranes for 45 min, cells were fixed and imaged using spinning disk confocal microscopy and the amount of ephrinA1 inside each cell was quantified (see Methods). Small corrals inhibited ephrinA1 trans-endocytosis, while internalization was successful on unrestricted substrates (Figure 3.7 *A*). The number of punctate ephrinA1 spots inside of cells on substrates with 1, 3, 5, and 10 µm corrals revealed a significant decrease in the amount of endocytosis on 1 and 3 µm grid sizes (Figure 3.7 *B-C* and Figure 3.8). Each cell encountered approximately the same amount of ephrinA1 protein, indicating that introducing a spatial and mechanical disruption of EphA2–ephrinA1

movement regulates trans-endocytosis. As a control, transferrin uptake in cells encountering patterned supported membranes with ephrinA1 was also monitored, and we observed no significant change in the uptake of transferrin across the different grid sizes (Figure 3.9).

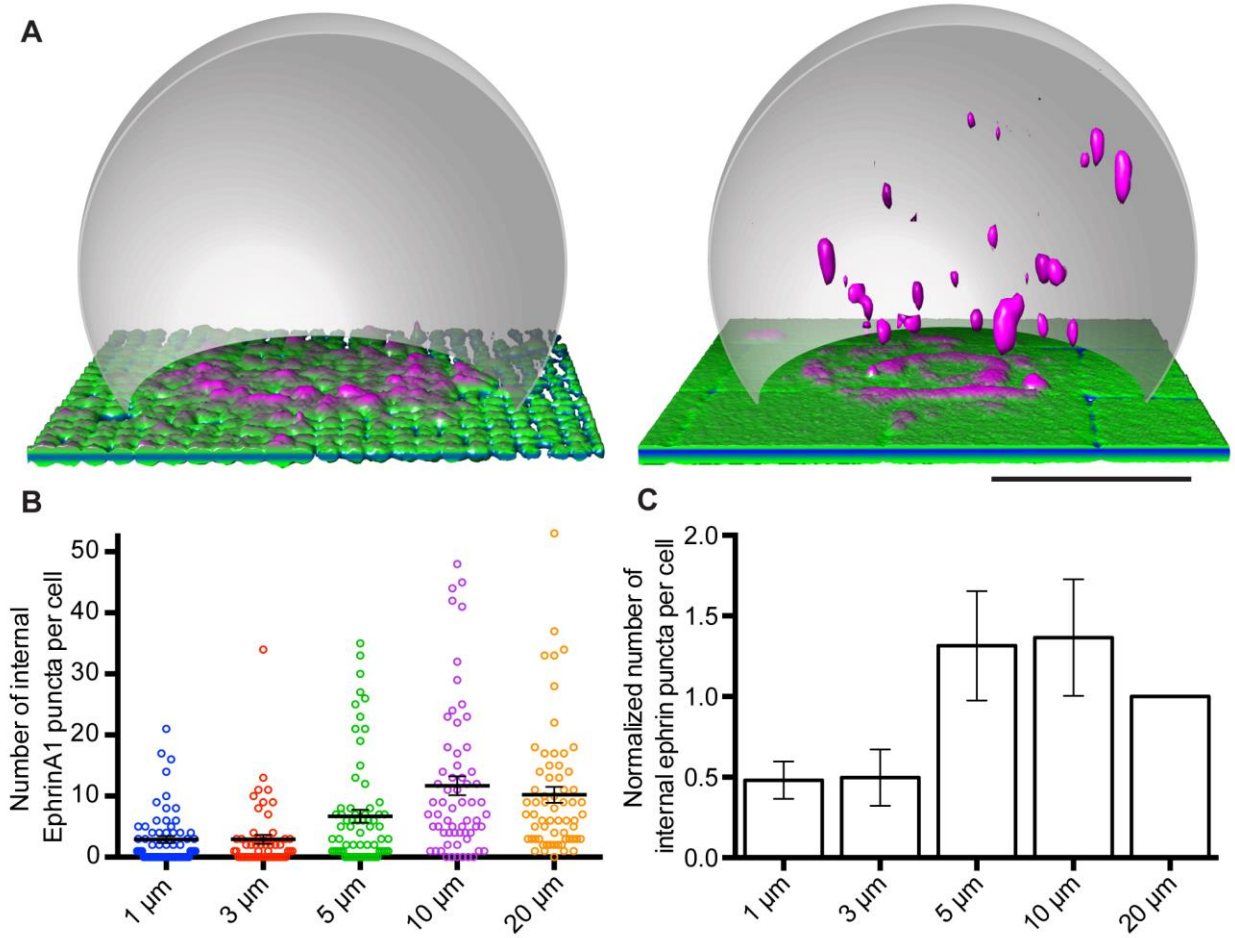

Figure 3.7 Spatiomechanical inhibition of EphA2-ephrinA1 endocytosis. A) Fixed MDAMB231 cells on supported membranes that are mechanically restricted by 1 mm (left) or 10 mm (right) grids. On small grid pitches, cells generally exhibited fewer internal ephrinA1 puncta, indicating less endocytosis from the interface. Images are 3D renderings of confocal fluorescence data of ephrinA1 labeled using Alexa Fluor 647 (pseudocolored as in Fig X) and a gray dome approximating the cell outline. Scale bar is 10 mm. B) Column scatter graph showing the amount of internalized ephrinA1 in each cell for one representative sample, which contained all grid patterns (e.g., 1, 3, 5, 10, and 20 mm or off grid). Bars are mean5standard error of the mean. n >50 cells on each grid pitch. Note that for 1 and 3 mm, >40% of the cells contain zero puncta (see Fig X). C) The result of multiple independent repeats of the representative sample shown in B. Values were first normalized to 20 mmin each sample, the normalized values at each grid pitch were then averaged across all samples. Error bars are standard error of the mean, n ¼ 6 samples, each with hundreds of cells. P<0.05 between 1 and 10 mmgrid pitch using ratio paired t-test.

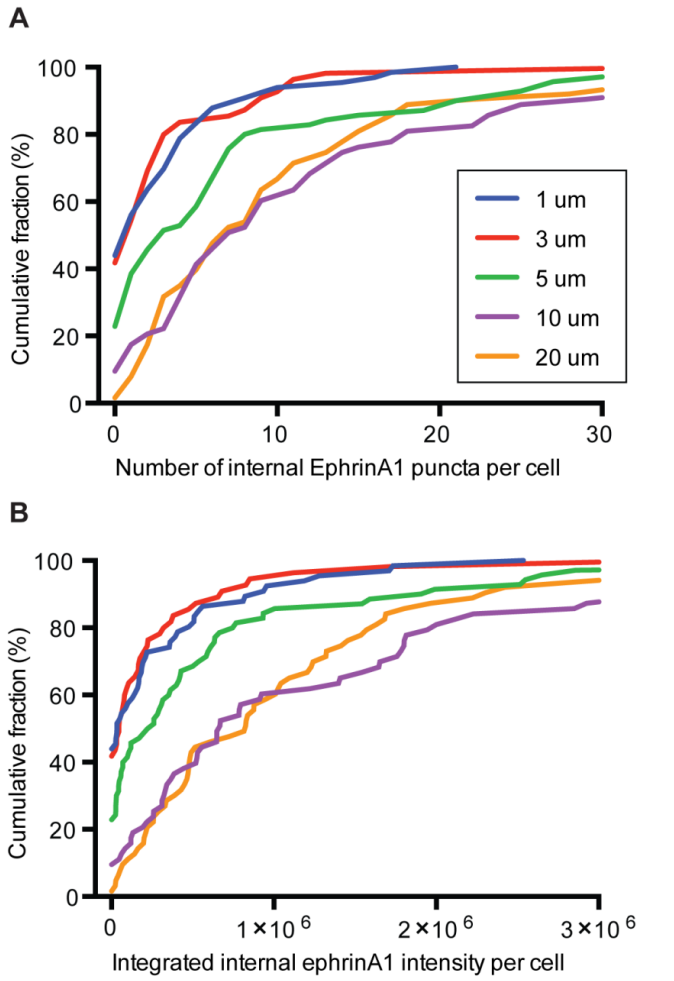

Figure 3.8 Empirical cumulative distribution plots of the number of A) ephrinA1 puncta (same data from Fig. 4*B*) and B) total ephrinA1 intensity within all the puncta in each cell. The overall distributions in both graphs are very similar, reaffirming that simply counting puncta is a reasonable measure of ephrinA1 internalization. (Each plotted line is effectively the integration under a histogram with infinitely small bin size.) Plots shifted to the right indicate a shift in the distribution to larger values. Note that for 1 and 3 µm, more than 40% of the cells contain zero puncta.)

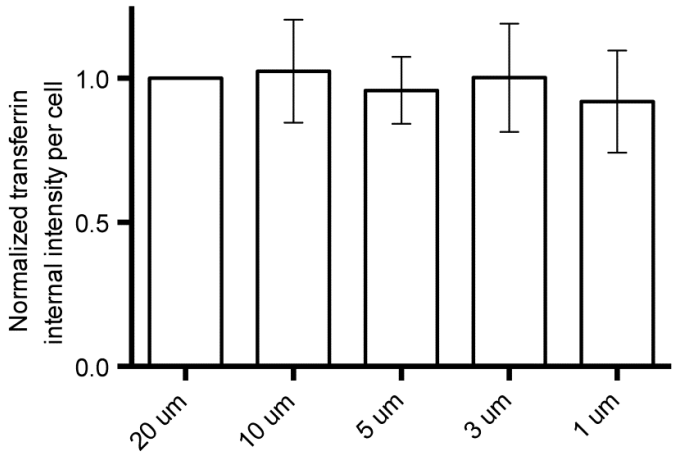

Figure 3.9 Transferrin uptake during spatio-mechanical inhibition of EphA2-ephrinA1 endocytosis. Experiment was performed as in Fig. 4 but with the addition of 25 µg/mL of labeled transferrin. Uptake was quantified as described in the methods, with the total internal intensity summed. Transferrin internalization was averaged across multiple samples. Each sample contained multiple repeats of each grid pattern (e.g. 1, 3, 5, 10, and 20 µm). Values were first normalized to 20 µm in each sample, then the normalized values at each grid pitch were averaged across all samples. Error bars are standard error of the mean, n = 4 samples, each with tens to hundreds of cells. The ratio paired t test revealed no

Section 3.3.4: Trans-endocytosis of ephrinA1 requires clathrin and ADAM10

We then asked whether targeted inhibition of the molecules that colocalize with EphA2–ephrinA1 alters ephrinA1 endocytosis. Cells were treated with the small molecule Pitstop2 to inhibit the clathrin terminal domain[105,106]. Treatment resulted in a significant decrease in ephrinA1 endocytosis, corroborating that EphA2–ephrinA1 is internalized through a clathrin-mediated endocytosis mechanism (Figure 3.10 *A*). These results indicate that EphA2 must be first bound to ephrinA1, phosphorylated and then actively internalized, consistent with recent work using soluble, dimeric ephrinA1. Interestingly, the localization of clathrin, dynamin, and caveolin did not differ dramatically for cells on 1 versus 10 μm gridded substrates (Figure 3.10 *A*-*B*), indicating that EphA2 sensitivity to grids is not simply caused by a change in recruitment of endocytosis molecules.

Because ADAM10 cleaves ephrinA1 and breaks the mechanical linkage to the underlying supported membrane, the metalloprotease may regulate EphA2–ephrinA1 internalization[50]. Our prior results indicated that ADAM10 recruitment is significantly reduced in cells on small grids[27], so we hypothesized that the mechanical sensitivity of EphA2–ephrinA1 endocytosis may be related to modified ADAM10 recruitment on grids. We treated cells with the small molecule INCB003619 to inhibit cleavage[107,108] of ephrinA1 by ADAM10 or ADAM17 (Figure 3.10 *B*) and found that inhibiting metalloprotease activity significantly reduced the amount of ephrinA1 inside the cells. This result was consistent with our hypothesis that cleavage of ephrinA1 is required for efficient internalization of the EphA2–ephrinA1 complex, as well as recent work suggesting that ADAM10 is required for trans-endocytosis of Eph receptors[50].

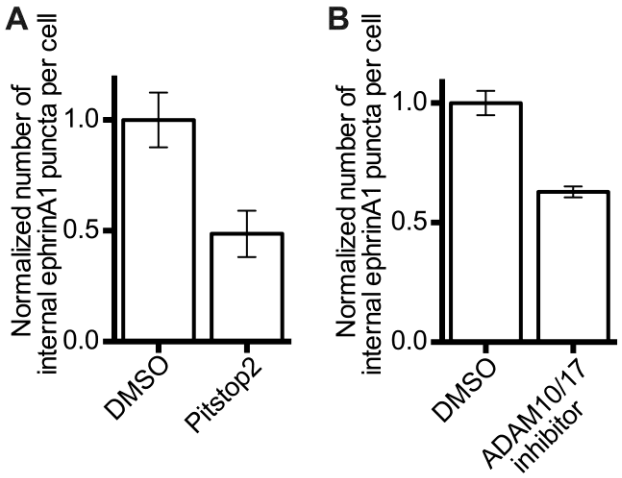

Figure 3.10 Drug inhibition of ephrinA1 trans-endocytosis. A) Blocking the clathrin terminal domain with the small molecule Pitstop2 reduces overall ephrinA1 endocytosis. Bars are mean5 SE, n ¼ 3 samples each condition, with >1000 cells per sample. P < 0.05 using the unpaired t-test. B) Inhibiting ADAM10 and ADAM17 metalloprotease activity using the small molecule INCB003619 reduces overall ephrinA1 endocytosis. Bars are mean5range, n ¼ 2 samples each condition, with ~1000 cells per sample. P < 0.05 using the unpaired t-test.

Section 3.4: Discussion

Our results indicate that EphA2 signaling and endocytosis is sensitive to spatial and mechanical properties of the apposing cell on the scale of microns. Preventing ephrinA1—and, indirectly, of EphA2—from forming large-scale clusters inhibits endocytosis. This represents a noncanonical mechanical sensitivity, because the cells are responding not to adhesion machinery (integrin

ligands are not present in the supported membrane) but instead to forces directly influencing an RTK[27].

We also found that chemically inhibiting ADAM10 reduces trans-endocytosis of ephrinA1. Whether ADAM10 recruitment is the primary regulator of EphA2–ephrinA1 internalization remains to be shown: loss of ADAM10 recruitment to small sites of EphA2–ephrinA1 contact may be a result of failed endocytosis instead of the cause.

It is possible that cells on physically restrictive substrates exhibit a systemic shift to a different signaling state, such as changing from a cell rounding behavior on fluid bilayers to a cell spreading phenotype on gridded substrates, which would be corroborated by our observation of altered cytoskeletal arrangement on gridded substrates[27]. However, our transferrin-uptake results (Figure 3.8) indicate that modulating EphA2–ephrinA1 spatial organization does not redefine the entire endocytosis machinery of the cell, even though transferrin also uses a clathrin-mediated endocytosis mechanism[109].

Alternatively, clathrin itself may be responding to the mechanical properties of EphA2–ephrinA1 contact sites or the curvature of the cell membrane. A gridded substrate imparts a pattern on the cell membrane only indirectly, via the cell's EphA2 bound to corralled ephrinA1 in the underlying patterned supported membrane. The smallest grid size used in this paper (1 μm) is sufficiently larger than the size of a clathrin-coated vesicle (~100 nm)[32,110], but the small grids result in drastically smaller ephrinA1–EphA2 clusters (Figure 1.1 *C*). Our colocalization results indicate that clathrin is still recruited on all grid pitches (Figure 3.11 *A-B*), but endocytosis is not as efficient on 1 and 3 μm grids. It is possible that there is a cluster-size threshold for effective endocytosis.

Besides the obvious factor of cluster size, ephrinA1 patterning may cause impeded endocytosis in other ways. Recent work[111] found that clathrin pit maturation may be impeded by membrane tension. The smaller grid sizes may introduce far more bending[112] in the cell membrane or increased tension reducing efficient pit maturation relative to the larger grid sizes. Furthermore, the cell membrane should exhibit lower local curvature or undulations when EphA2–ephrinA1 complexes are allowed to freely coalesce to large contacts site versus the case where they are corralled by small grids[113,114]. This altered membrane curvature[79,115], or possibly even impeded flow of cell membrane lipids[115], may inhibit pit formation or maturation . These mechanisms remain to be explored.

An argument could be made that our results are simply due to a decrease in concentration of ephrinA1 on smaller grid sizes, thereby reducing the amount of material available to be internalized. For instance, regulation of epidermal growth factor receptor (EGFR) endocytosis occurs via two distinct mechanisms, and the balance between the two pathways is determined by the ligand concentration[116]: at very high concentrations of the ligand EGF, non-clathrin mediated endocytosis takes on a larger role (likely because the clathrin machinery is saturated). However, we do not believe our findings were the result of such an effect. First, the grids are barriers to lipid and protein diffusion, but they do not change the protein concentration; therefore, the number of ephrinA1 molecules available to a cell is approximately the same

across the different grid sizes. Second, while we did observe some variability in the brightness under different cells, that variability did not correlate with grid pitch. Finally, we found no evidence for significant concentration dependence: we observed only a very weak correlation between ephrinA1 concentration and material internalized (Figure 3.2). Instead, the grids primarily disrupt *local* concentration (i.e. clustering); therefore, we propose that endocytosis is strongly influenced by the large-scale clustering of the RTK–ligand at the cell–membrane interface.

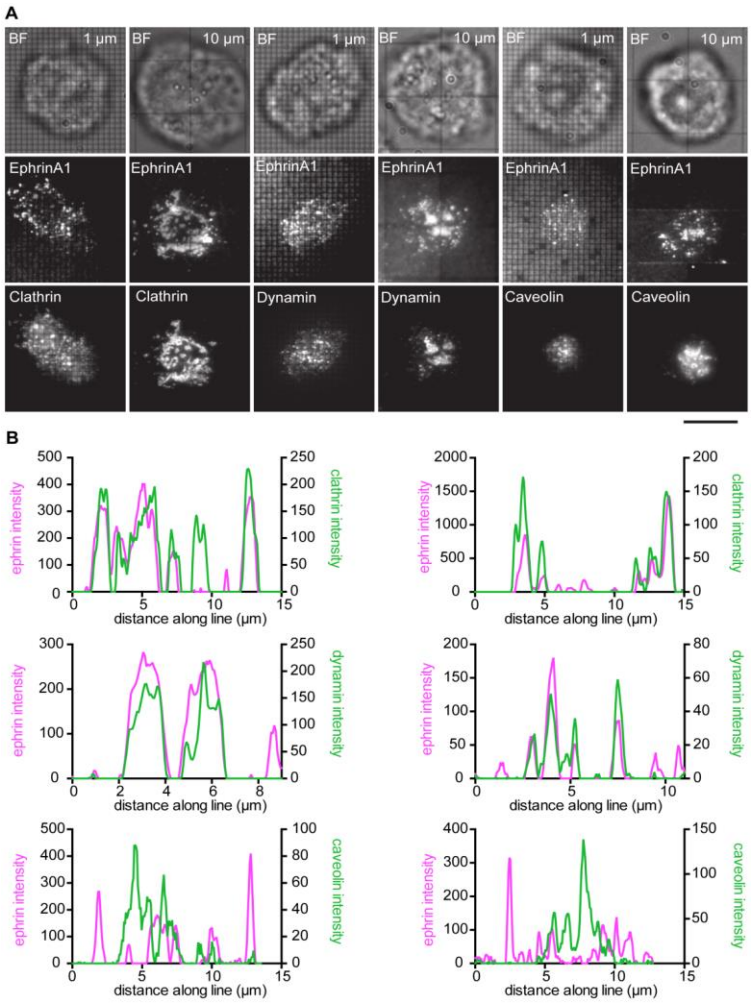

Figure 3.11 Recruitment on grids. A) Epifluorescence images of single cells transiently expressing the indicated signaling molecule on a fluorescent ephrinA1 bilayer with either 10 or 1 μm gridded substrates. B) Line profiles of ephrin intensity overlayed with clathrin, dynamin, or caveolin intensity. Colocalization type did not qualitatively change from unrestrained bilayer or for cells on 10 (*left*) or 1 μm (*right*) gridded substrates. Clathrin and dynamin still gets recruited to the ephrin cluster, regardless of size; caveolin is excluded from ephrin clusters. Background was removed by subtracting a version of the image that was blurred with a 25 pixel Gaussian kernel.

To our knowledge, this is the first report of a quantitative trans-endocytosis assay of ligands on a supported membrane, which mimics a cell–cell junction. These results in conjunction with several recent findings [27–29,47,117,118], support an emerging theme in which receptor movement and large scale clustering during cell–cell contact dramatically alters how cells signal. This effect ranges from proximal signaling events, such as recruitment of proteins to the membrane, to far-downstream signaling events such as endocytosis. Understanding this regulatory component in greater detail can provide insight into how receptor movement and reorganization might contribute aberrant signaling in cancer, especially in tumors that highly overexpress the EphA2 receptor[119].

Chapter 4

Section 4.1: Introduction

Section 4.1.1: EphA2 pathology

EphA2 has been shown to be highly overexpressed in many aggressive cancers including breast cancer [120] and often found in triple negative breast cancers, including MDAMB231 cells. The triple negative class of breast cancers lack the expression of the progesterone receptor, the estrogen receptor and Her2, all of which have targeted chemotherapy treatments, making EphA2 an important target in the development of novel direct chemotherapires. Unlike many other receptor tyrosine kinase misregulations, however, EphA2 is only rarely found to be mutated in cancer[121]. Studies indicate that the oncogenic transformation of the EphA2 receptor is not a result of a chemical mutation in protein sequence, but rather a *functional* alteration that allows the receptor to escape phosphorylation and subsequent degradation by the c-Cbl adaptor protein complex[122,123]. Overexpression of nonmutated EphA2 has even been found to be sufficient to induce tumorigenesis and metastasis in nontransformed mammary epithelial cells[18], and is associated with poor patient prognosis[23]. While some EphA2 mutations have been identified, most of these occur in the SAM domain and are associated with cataract disease[124,125].

Section 4.1.2: EphA2 structure and clustering

EphA2 is a 976 amino acid length protein with an extracellular region consisting of a ligand-binding domain, a cysteine-rich domain which is divided into a sushi domain and an epidermal growth factor-like domain and two fibonectin III repeats followed by a transmembrane region of the protein and intracellularly, a juxtamembrane region, a kinase domain, a sterile alpha motif (SAM) and a PDZ domain[126]. Eph receptor activation does not seem to follow the canonical RTK dimerization model; rather, Eph activation causes oligomerization resulting not only from Eph–ephrin interactions, but also Eph *cis* interactions mediated through the sushi[9,10] and SAM domains[11] of the Eph receptor. This in turn can propagate ligand-mediated seeding or oligomerization of Eph receptor clusters that is not dependent upon direct ephrin contact[12]. Structural studies confirm that Eph–ephrin clustering is not consistently a direct 1:1 stoichiometry of receptor to ligand binding[9,13]. Additionally, Eph signaling is further complicated by the ability of the receptor to signal in both a ligand-dependent and ligand-independent

manner[14]. Together, misregulation of these unique features of both Eph signaling and clustering likely play a role in disrupting the fine-tuning and balance of appropriate Eph receptor signaling in disease progression[15].

Section 4.1.3: EphA2 clustering and drug targeting

We previously showed that the disease-state of the cell correlates to the degree of EphA2 clustering[127]. By screening through a library of breast cancer cell lines using a hybrid display of static and fluid ephrinA1, we found that EphA2 clustering in invasive and metastatic breast cancer cells was highly altered relative to the more benign cancer cell lines. These results suggest that there likely exist strong Eph *cis* receptor associations that may correlate to the pathological misregulation of Eph signaling[127].

Recently, an antibody-drug conjugate, MEDI-547, targeting the EphA2 receptor was used in a Phase I trial treating six different cancer patients[128]. MEDI-547 was previously designed as a monoclonal antibody targeted against the EphA2 receptor conjugated to the microtubule inhibitor, auristatin. Preclinical studies in cell lines and in mouse models determined that MEDI-547 binds to EphA2, is internalized and induces apoptosis upon delivery of auristatin intracellularly[129]. When used in human cancer patients, however, the drug had extremely deleterious effects, including pain, hemorrhaging and liver disorder, causing the premature termination of the study. Auristatin has previously been used in other antibody-drug conjugates, suggesting that the toxicity of MEDI-547 was not due to auristatin. More likely, the extreme toxicity can be contributed to the monoclonal EphA2 antibody. Precisely what went wrong in the phase I trial, however, is not well understood.

It is possible that the pathological results of the phase I drug trial might be a result of increased EphA2 clustering via the antibody portion of MEDI-547. MEDI-547 likely altered not only the balance of ligand-dependent and ligand-independent EphA2 signaling, but also seeded increased EphA2 receptor clustering. While the precise consequences of disrupting either of these aspects of EphA2 signaling has not been explored in detail, it is possible that inducing clustering using MEDI-547 resulted in a more pronounced disease state, similar to our previous findings.

Recent work done by the Jones lab found that two point mutations in the EphA2 sushi dimerization interface, which mediates Eph-Eph *cis* interactions, results in a decrease in EphA2 clustering, even upon ephrinA1 stimulation in solution[13]. More importantly, they discovered that these EphA2 mutants alter intrinsic downstream signaling events, presumably only due to changes in EphA2 clustering. How a single point mutation that disrupts receptor-receptor *cis* interactions alters cell signaling, even upon ligand activation, is not well understood. Being able to directly observe EphA2 clustering and understand how the sushi domain mediates EphA2 clustering will not only provide greater biophysical understanding of EphA2 clusters, but also information for how to design effective chemotherapies targeting EphA2.

Here, we address this question by using a variety of microscopy techniques to directly observe EphA2 clustering and determine the role of the sushi domain in this large-scale clustering process. By using super resolution microscopy techniques, such as stochastic optical reconstruction microscopy (STORM), we can define these clusters at a much greater resolution than previously detected, allowing us to determine receptor-ligand stoichiometry as well as cluster density. Understanding how EphA2 clustering is regulated can provide insight into effective strategies for targeting the receptor for treatment.

Section 4.2: Materials and Methods

Section 4.2.1: Protein expression, purification, and labeling

The soluble, monomeric human ephrinA1 sequence (gift of Hans-Christian Asheim, Oslo University, Norway) modified with a C-terminal decahistadine tag (gift of Qian Xu) was cloned into the pFastBac™1 (Invitrogen, Carlsbad, CA) expression cassette. The expression cassette was transformed into DH10Bac™ *Escherichia coli* cells (Invitrogen, Carlsbad, CA) and DNA was purified to obtain recombinant viral DNA bacmid. SF9 cells (gift of Ann Fischer, UC Berkeley, CA) were transfected with the bacmid DNA using Cellfectin II (Invitrogen, Carlsbad, CA) to generate recombinant baculovirus followed by amplification of viral stocks. SF9 cells were grown in serum-free Sf-900 II SFM insect cell medium and four liters of mid-logarithmic growth phase cells were infected with 50 mL of P2 baculovirus. Cells were centrifuged at 6000 x g and the supernatant containing soluble ephrinA1-H10 was purified using a gravity flow column containing Ni^{2+}-NTA agarose (Qiagen, Valencia, CA). The ephrinA1-H10 was then covalently labeled with an Alexa Fluor 647 antibody labeling kit (ephrinA1-647) per manufacturer's instructions (Invitrogen, Carlsbad, CA).

Section 4.2.2: Supported membrane assembly

Vesicles composed of 98 mol% 1,2-dioleoyl-*sn*-glycero-3-phosphocholine (DOPC) and 2 mol% of 1,2-dioleoyl-*sn*-glycero-3-[(N-(5-amino-1-carboxypentyl)iminodiacetic acid) succinyl] (nickel salt) (Ni^{2+}-NTA-DOGS) (Avanti Polar Lipids, Alabaster, AL) were made according to standard procedures[54]. Hydrated lipid vesicles were extruded through a 100 nm membrane eleven times, and then a 30 nm polycarbonate membrane three times using an Avanti Mini-Extruder (Avanti Polar Lipids, Alabaster, AL). Supported membranes were then formed on #1.5 Warner brand 25 mm round coverslips according to standard procedures[54]. The supported membrane was then enclosed in an Attofluor cell chamber (Invitrogen, Carlsbad, CA). Membranes were blocked with 1 mg/mL casein solution prior to incubating them with 10 nM ephrinA1-H10 for 1.5 hours according to published methods[52]. Excess protein was thoroughly rinsed away and the membranes were then rinsed with HEPES buffered saline (see below) with 10% fetal bovine serum (Thermo Scientific, Logan, UT) prior to the addition of cells. (Other cell media, especially DMEM with 10% fetal bovine serum, contained ingredients that significantly interfered with the nickel chelation of the His-tagged ephrinA1, causing the protein to detach from the membrane

within minutes at 37°C. In HEPES buffered saline with 10% fetal bovine serum, the His-tagged linkage to the membrane was stable for many hours.)

Section 4.2.3: Hybrid display of immobile RGD and fluid ephrinA1

RGD repeat peptide patterns were fabricated on 25 mm diameter round glass coverslips, which were cleaned for 10 minutes in using a plasma cleaner (Figure 4.3). Clean coverslips were incubated with 250 µg/mL of PLL-PEG-Biotin (SuSoS, AG, Switzerland) polymers for 120 minutes followed by rinsing in distilled water and drying. A previously designed photomask (by Zhongwen Chen at the Molecular Biology Institute at the University of Singapore) was exposed to deep UV for 5 minutes to clean the surface followed by rinsing in distilled water and drying. The mask contains patterns of varying shapes (squares or circles) and sizes (~1.8 µm – 5 µm). A small drop of distilled water was added on to the desired pattern of the photomask and the dried PLL-PEG-Biotin surface-coated coverslip was laid upon the water droplet, creating a tight contact with the photomask. The photomask was exposed to deep UV for 7.5 minutes, effectively degrading the polymer where not shielded from the photomask as well as creating a hydrophilic surface for the formation of a supported lipid membrane. The coverslip was removed by copious flushing with water, dried and the vesicles were added to the coverslip to form a membrane as described above. Bilayer-RGD substrates were blocked with 1 mg/mL casein for 30 minutes. 1.5 µg/mL neutravidin-cascade-blue (Invitrogen, Carlsbad, CA) was incubated with 10 nM ephrinA1-H10 for 30 minutes, following by rinsing with TBS. 1.5 µg/mL Biotin-RGD (Peptides Int, Louisville, KY) and 10 nM ephrinA1-H10 were then added and incubated for an additional 60 minutes, following by rinsing with TBS.

Section 4.2.4: Cell culture and transfection.

HeLa cells (gift of Ann Fischer, UC Berkeley, CA) were cultured in DMEM with Glutamax (Invitrogen, Carlsbad, CA) supplemented with 10% fetal bovine serum (Thermo Scientific, Logan, UT). Cells were stripped from culture flasks using Cellstripper (Mediatech, Manassas, VA) and resuspended in 1x HEPES buffered saline (20 mM HEPES, 137 mM NaCl, 5 mM KCl, 0.7 mM $Na_2HPO_4 \cdot 7H_2O$, 6 mM D-glucose, 1 mM $CaCl_2 \cdot 2H_2O$, 2 mM $MgCl_2 \cdot 6H_2O$) with 10% fetal bovine serum for experiments. Cells were rinsed with 1x Dulbecco's PBS prior to changing the cell medium to low-serum Opti-MEM (Invitrogen, Carlsbad, CA). Following manufacturer's instructions, cells were transfected with 10 µg of DNA using the Neon electroporation system (Invitrogen, Carlsbad, CA). The DNA construct of EphA2 (or the EphA2 sushi domain mutant) fused to an mCherry was used previously and is a gift of the Jones Lab[13].

Section 4.2.5: Genome editing

MDAMB231 cells (gift of Ann Fischer, UC Berkeley, CA) were cultured in DMEM with Glutamax (Invitrogen, Carlsbad, CA) supplemented with 10% fetal bovine serum (Thermo Scientific, Logan, UT). Genome-editing was performed using the CRISPR Cas9 system and protocols were following according to published methods[130]. Guides were designed using the online CRISPR

design tool (http://crispr.mit.edu/). Two guides were chosen and cloned into the pCas9-2A(BB)-GFP expression plasmid (gift of Jennifer Doudna, UC Berkeley, CA). The donor DNA was designed as a 200bp single strand DNA oligo containing the two point mutations of interest and synthesized (Integrated DNA Technologies, Inc., Coralville, IA). Donor DNA and the Cas9 expression plasmid with the confirmed guide RNA sequence was transfected into MDAMB231 cells using Lipofectamine 2000 (Invitrogen, Carlsbad, CA) for 5-8 hours according to standard protocols. Cells were sorted 24 hours later to isolate single cell clones positive for GFP. Single cells were expanded and screened for the genome-edited point mutation.

Section 4.2.6: Total internal reflection fluorescence (TIRF) and stochastic optical reconstruction (STORM) microscopy

All TIRF microscopy hardware was controlled with and images were acquired using Micro-Manager [100]. Microscopy was performed on a motorized inverted microscope (Nikon Eclipse Ti-E/B, Technical Instruments, Burlingame, CA) equipped with a Nikon 100x Apo TIRF 1.49 NA objective lens, motorized Epi/TIRF illuminator, motorized Intensilight mercury lamp, Perfect Focus system, and a motorized stage (ASI MS-2000, Eugene, OR). Lasers included the following: 200 mW 488 nm Ar-ion laser (Spectra Physics 177G, Santa Clara, CA), 100 mW 561 nm optically-pumped solid state laser (Coherent Sapphire, Santa Clara CA), and 100 mW 640 nm diode laser (Coherent Cube, Santa Clara CA). Lasers were controlled using an acousto-optic tunable filter (AOTF) and aligned into a dual-fiber launch custom built by Solamere (Salt Lake City, UT): one single-mode polarization maintaining fiber (Oz Optics, Ottawa, Canada) was connected to a TIRF illuminator, while the other was connected to the spinning disk confocal unit.

TIRF, reflection interference contrast microscopy (RICM), and bright field images were collected using a 1024×1024 pixel electron-multiplying CCD camera (Andor iXon3 888, Belfast, Ireland), typically at gain setting 200 and with pixels binned 2×2 for higher signal-to-noise. Dichroics were 2 mm thick and mounted in metal cubes to preserve optical flatness: ZT488rdc, ZT561rdc, and ZT640rdc. Long-pass emission filters included: ET500lp, ET575lp, and ET660lp. Bandpass emission filters were located below the dichroic turret in a motorized filter wheel (Sutter Lambda 10-3, Novato CA): ET525/50m, ET600/50m, and ET700/75m. RICM was performed using a 50/50 beamsplitter with a D546/10x filter. All TIRF filters and dichroics were from Chroma (Bellows Falls, VT).

Live-cell imaging was performed using a stage-top incubator and objective heater (Chamlide TC-A, Quorum Technology, Guelph, Canada).

Samples for STORM were prepared as mentioned above and fixed with ultra-pure 4% paraformaldehyde (Polysciences, Warrington, PA) in 1x PBS for 15 min followed by a 10 mL 1x PBS rinse. All STORM microscopy data was taken in collaboration with Professor Ke Xu and his graduate student, Samuel Kenney (UC Berkeley).

Section 4.2.7: Image Analysis

Figure 5.5 was created using PDB structures in Pymol and arranged in Adobe Illustrator. The following PDB files were used: EphA2:ephrinA5 PDB ID: 2X11 [55].

Section 4.3: Results

Section 4.3.1: EphA2 sushi domain mutants cluster faster than the wildype

To directly observe EphA2 clustering and determine the role of the sushi domain in this large-scale clustering process, we transiently expressed EphA2 fused to mCherry in live HeLa cells, which do not natively express EphA2. We used either a wildtype EphA2 or a mutant with two point mutations in the sushi domain creating an N-linked glycan residue (gift of the Jones lab, Oxford). The advantage of using HeLa cells is that the expressed EphA2 (whether wildype or mutant) is not being expressed in a background of endogenous EphA2 receptors. The only EphA2 being activated is the EphA2 that is transiently expressed in the cells. We then culture these EphA2-expressing cells on a supported lipid membrane displaying mobile ephrinA1 ligands. We first observed differences in clustering between the mutant EphA2 on an ephrinA1-displaying supported lipid membrane using total internal reflection fluorescence (TIRF) microscopy. Live-cell timelapse microscopy images revealed that a mutation in the sushi domain of the EphA2 receptor results in faster clustering of ephrinA1 on a supported membrane (Figure 4.1). The intensity of ephrinA1 and the number of ephrinA1 clusters formed increased at a much faster timescale in the mutant compared to the wildtype.

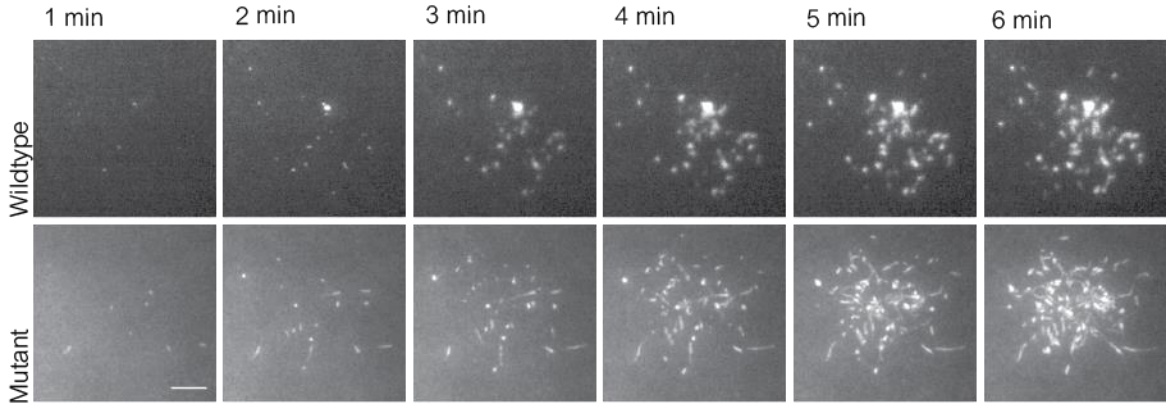

Figure 4.1 HeLa cells expressing either wildtype or mutant EphA2 interacting with a mobile ephrinA1-displaying supported membranes. TIRF microscopy timelapse of single cells clustering ephrinA1-647. Scale bar is 5 µm.

We then sought to determine the structure and stoichiometry of the EphA2-ephrinA1 clusters using high resolution microscopy. We prepared the samples and allowed the cells to engage with the ephrinA1-displaying membrane for 5 minutes prior to fixation. Samples were then prepared for STORM imaging in collaboration with the Xu lab. Both the EphA2 receptor and the

ephrinA1 ligand were imaged separately for wildype and mutant samples. Samples were prepared in which the Alexa Fluor 647 label was on ephrinA1 and the receptor remained unlabeled, or the ephrinA1 remained unlabeled and EphA2 was labeled with a nanobody against the mCherry fusion protein conjugated to Alexa Fluor 647. Even at early clustering time point, STORM data revealed that the EphA2-ephrinA1 clusters were too dense to resolve using super-resolution microscopy (Figure 4.2).

Section 4.3.2: Hybrid display of immobile RGD and mobile ephrinA1

These data prompted the development of an assay in which ligand density could be physically limited in order to resolve cluster structures and stoichiometry. Imaging also revealed "line-like" cluster structures being formed (Figure 4.1 and 4.2). As cells engage an ephrinA1-displaying membrane, they begin to round due in part to the physical engagement of ligands on a supported membrane. To reduce any imaging artifacts due to intrinsic cell-rounding, we sought to develop an assay in which ligand density can be restrained and integrin proteins on the cell surface are engaged with the purpose of flattening out the cells. To do this, we coat coverslips with a PLL-PEG-Biotin polymer and use photolithography to etch away patterns of particular designs to create regions of clean, exposed glass in which mobile supported membranes can be formed (Figure 4.3 *A*). This allows for functionalization of RGD repeat peptides (which will bind to and engage integrin ligands in the cell) on the immobile PLL-PEG-Biotin, as well as fluid ephrinA1 on regions of mobile supported lipid membranes, creating a hybrid display of immobile RGD and mobile ephrinA1 (Figure 4.3 *B*). This unique fabrication technique allows for ephrinA1 density to be physically confined, as well as engaging integrin ligands to decrease cell-rounding artifacts.

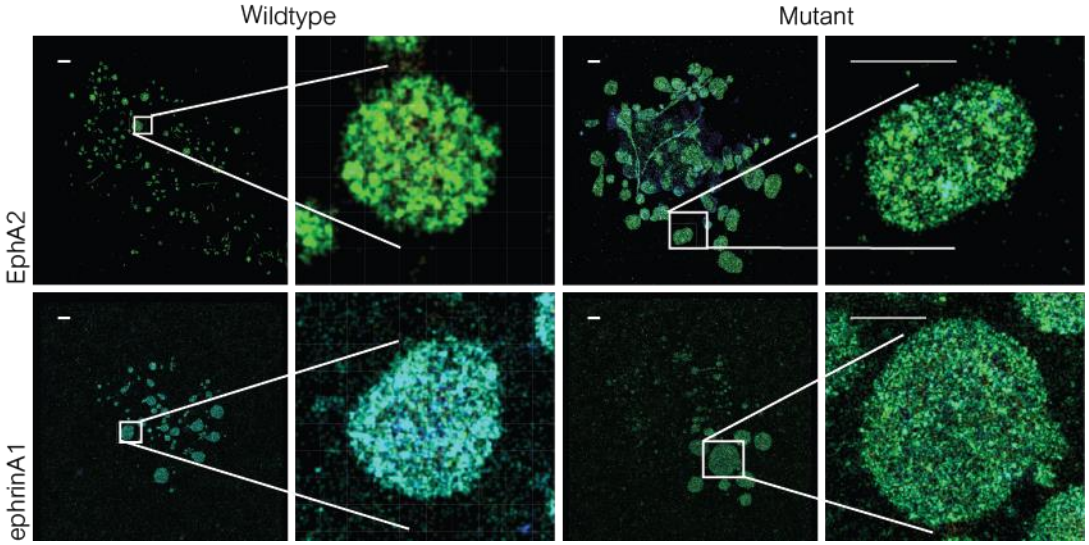

Figure 4.2 HeLa cells expressing either wildtype or mutant EphA2 interacting with a mobile ephrinA1-displaying supported membranes. STORM microscopy images single cells clustering ephrinA1-647. Receptors were labeled in one sample and ligands were labeled in a separate sample. Each image has a cluster that is zoomed in on to reveal more detailed information. Scale bar is 1 μm.

We then repeated both our TIRF and STORM imaging experiments using a hybrid display of RGD and ephrinA1. TIRF microscopy revealed that the sushi domain EphA2 mutation results in faster clustering and more transient cluster formation of ephrinA1 on a supported membrane (Figure 4.4). The intensity of ephrinA1 and the number of ephrinA1 clusters formed increased at a much faster timescale in the mutant compared to the wildtype. The wildtype clusters formed at a slower rate and remained more clustered over the imaging time.

STORM was repeated using a 2-color approach in which the EphA2 receptor was labeled with a nanobody conjugated to Alexa Fluor 647 and the ephrinA1 ligand was conjugated to a Cy3b dye. The Cy3b dye had fewer switching events and was not as easily aligned, limiting the amount of structural information gained from these data. Future STORM imaging experiments include repeating these experiments using one-color STORM of the receptor and ligand independently on a hybrid display of ephrinA1 and RGD.

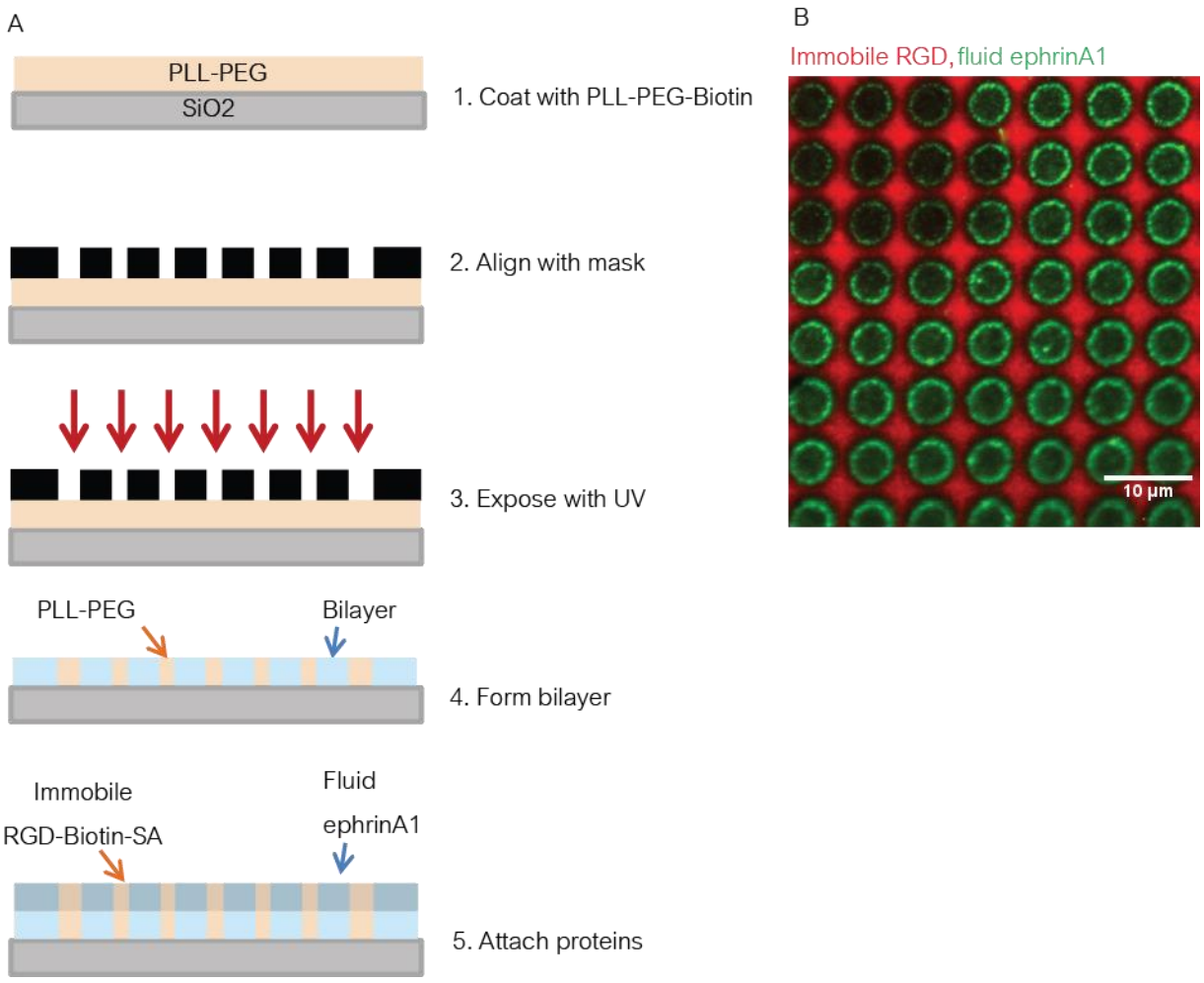

Figure 4.3 Hybrid display of immobile RGD and mobile ephrinA1. A) Schematic for photolithography fabrication technique used. PLL-PEG was coated onto a glass surface and aligned with the photomask. The coverslip was then exposed to deep UV and supported lipid membranes were subsequently formed. RGD was attached to the immobile patterns of PLL-PEG and ephrinA1 was attached to the fluid supported membranes. B) Epifluorescence image overlay showing the RGD patterns in red and the fluid ephrinA1 supported membranes in green. A fluorescence recovery after photobleaching (FRAP) experiment was performed on the top left corner of the substrate. If the ephrinA1 ligand was immobile, distinct lines from the closed aperture would be evident. The lack of any distinct aperture shape indicates that ephrinA1 is mobile.

While understanding structural information of EphA2-ephrinA1 clustering will provide many insights into how clustering regulates the signaling process, we are likewise interested in downstream signaling effects of the cluster mutant and how this might alter the disease state of the cell. Studying downstream signaling in cells that do not endogenously express EphA2 does not provide the appropriate context since these cells may not have the suitable signaling machinery to signal through the EphA2 pathway.

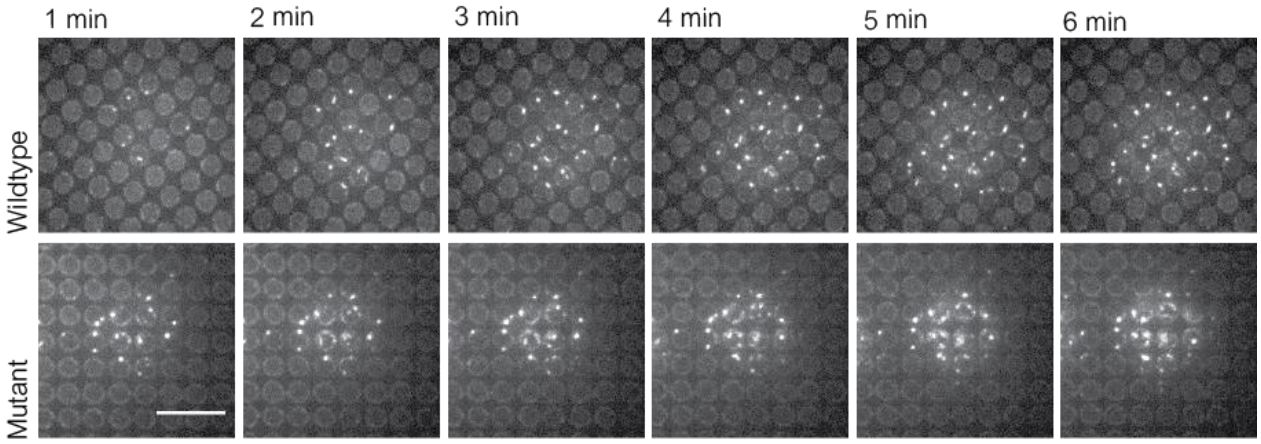

Figure 4.4 HeLa cells expressing either wildtype or mutant EphA2 interacting with a hybrid display of immobile RGD and mobile ephrinA1 on supported membranes. TIRF microscopy timelapse of single cells clustering ephrinA1-647. Scale bar is 5 µm.

Section 4.3.3: Genome-editing the sushi domain mutations into MDAMB231 cells

These limitations motivated us to examine the effects of the cluster mutants in a context in which cells endogenously express the receptor. We chose to genome-edit the sushi domain point mutations into MDAMB231 cells, which will allow us to directly compare how the cluster mutant alters cell signaling in well-characterized cells that highly overexpress a non-mutated version of EphA2. We used the CRISPR Cas9 genome engineering system according to published protocols[130]. Donor DNA was designed as a single strand DNA oligo containing the two point mutations in the sushi domain. This oligo was co-transfected into cells with the Cas9 expression plasmid containing guide RNAs (and a GFP) designed to cleave near the point mutation site. Successful cloning of the guide RNA sequences was confirmed and cells were co-transfected with the Cas9-guide RNA plasmid and the donor single strand DNA oligo. Cells were sorted based upon GFP expression (indicating that the expression plasmid was successfully transfected) and seeded as single cell clones into a 96-well plate. Single cell clones were allowed to expand for several weeks prior to screening for the insertion of the mutation.

Developing a cell line endogenously expressing an EphA2 mutation in the *cis* receptor clustering domain allows for huge advancements in understanding how the regulation of EphA2 clustering alters cell signaling and behavior, particularly in the context of metastatic breast cancers. The structure and stoichiometry of EphA2-ephrinA1 clusters as well as changes in cell behaviors, such as proximal membrane signaling and invasion potential, can be simultaneously monitored. Dual measurements of biophysical parameters and cell phenotypes will allow for great insights into how EphA2 clustering can regulate far downstream signaling events and how signaling is misregulated in different disease states.

Section 4.4: Discussion

Our results currently point to a mechanism in which EphA2 exists in association with other EphA2 receptors in *cis* in an unligated state, perhaps forming a network of Eph receptors across the cell membrane. Activation of EphA2 by ephrinA1 requires an energy input to break and rearrange the EphA2 receptor interactions resulting in a moderately fast observed clustering of ephrinA1 ligands (Figure 4.5). This model is supported by the sushi domain mutant data in which abolishing EphA2 *cis* interactions by introducing two point mutations in the sushi domain result in significantly increased rate of clustering of ephrinA1 ligands. Unligated Eph *cis* interactions are most likely mediated via the sushi domain, resulting in an intrinsic negative regulation of ephrinA1-mediated Eph-ephrin clustering, requiring a rearrangement of receptors upon ephrinA1 binding. Taken together, these experiments will provide insight into the importance of EphA2 *cis* clustering in the intrinsic EphA2 signaling pathway.

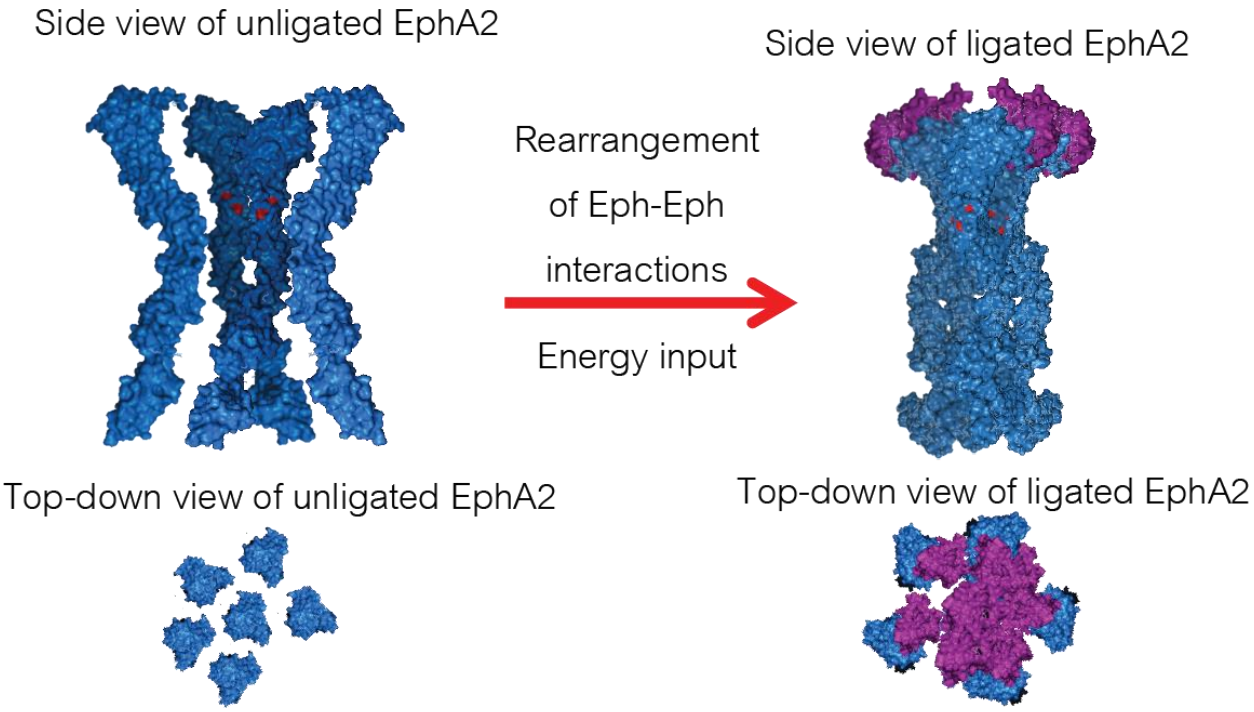

Figure 4.5 Model of how EphA2 *cis* interactions modulate EphA2 clustering. EphA2 interactions are mediated via the sushi domain. The two amino acids mutated in the sushi-domain mutant are colored in red. EphA2 likely interacts with other EphA2 receptors via this domain and forms a network of Eph *cis* interactions at the cell membrane. Activation of EphA2 by binding of ephrinA1 requires an energy input and rearrangement of EphA2 receptors to break this interactions and results in a more tightly clustered receptor-ligand complex.

Chapter 6: Closing Remarks

Understanding how the EphA2 receptor is regulated by space and mechanics, and the coupling of these two mechanisms, is key to understanding how Eph receptor signaling is misregulated in disease progression, particularly in cancer metastasis. We have just begun to scratch the surface in our knowledge that EphA2 is unique a RTK not only in its non-canonical signaling geometry, but also in how it clusters, both at the nanoscale and the micron-scale. Appropriate EphA2 signaling is a result of the proper balance between ligand-mediated and ligand-independent receptor signaling. How alterations in spatial organization and clustering at different length scales upset this fine-tuned balance of signaling is key to teasing apart how EphA2 becomes misregulated in disease. Until we have a firm understanding of the different regulatory features of the EphA2 signaling pathway, targeting the receptor in different drug therapies will remain extremely challenging.

Our work has revealed that EphA2 proximal membrane signaling is altered as a function of the spatial and mechanical properties of the apposing cell on the scale of microns. Recruitment of metalloprotease signaling molecules is altered when clustering is restricted, resulting in changes in far downstream signaling such as internalization[27,28,127,131]. This represents a noncanonical mechanical sensitivity of a receptor tyrosine kinase, because the cells are responding not to adhesion machinery (integrin ligands are not present in the supported membrane) but instead to forces directly influencing a receptor[27]. These results in conjunction with several recent findings [27–29,47,117,118], support an emerging theme in which receptor movement and large scale clustering during cell–cell contact dramatically alters how cells perceive their environment and signal in response.

We have also begun exploring the spatial organization of EphA2-ephrinA1 at the nanoscale. Structural studies indicate that EphA2 can form interactions (or clusters) not only with ephrinA1, but also with other EphA2 receptors. Having multiple domains to mediate clustering with both receptors and ligands results in complicated oligomerization. How oligomerization at the nanoscale alters ligand-mediated and ligand-independent signaling of EphA2 is not well understood. It is important to define the local densities of both the receptor and ligand in a living cell to connect how oligomerization directly affects cell signaling. We, and other researchers, have found that EphA2 receptors exist in association with other EphA2 receptors in *cis* in an unligated state. Eph c*is* receptor interactions likely form a network of Eph receptors across the cell membrane. Activation of EphA2 by ephrinA1 requires an energy input to break

and rearrange the EphA2 receptor interactions, mediated in part by the sushi domain of the receptor. Abolishing the sushi domain interactions results in an increased rate of clustering upon activation by membrane-bound ephrinA1 ligands. The EphA2 receptor seems to have an in intrinsic negative regulation of ephrinA1-mediated Eph-ephrin clustering, requiring a rearrangement of receptors upon ephrinA1 binding.

Taken together, we are beginning to understand the complex mechanisms by which EphA2 is regulated, from clustering and oligomerization at the structural level to large, micron-scale reorganization of EphA2-ephrinA1. How changes at the nanoscale directly impact cell signaling remains to be explored. We now have built a toolbox of reagents to answer these questions. Using genome-edited cells that endogenously express mutations in the EphA2 sushi domain will allow direct observations of how disrupting EphA2 *cis* clustering at the nanoscale impacts cell signaling. It also remains to be explored what went wrong mechanistically with the Phase I drug trial targeting EphA2. Furthermore, using our library of versatile ephrinA1 ligands allows us to address how EphA2 can signal in both a mechanically-dependent (from membrane-bound ephrinA1) and a mechanically-independent (from soluble ephrinA1) manner. All of these unique regulatory mechanisms render EphA2 an extremely complex receptor to decode. However, with the recent advances made in understanding Eph receptor signaling, it is an exciting time to continue studying EphA2 in more complex detail with hopes to effectively target the receptor in different drug treatments.

Bibliography

1. Lackmann, M. & Boyd, A. W. Eph, a protein family coming of age: more confusion, insight, or complexity? *Sci. Signal.* **1,** re2 (2008).

2. Adams, R. H. & Klein, R. Eph receptors and ephrin ligands. essential mediators of vascular development. *Trends Cardiovasc. Med.* **10,** 183–8 (2000).

3. Adams, R. H. *et al.* Roles of ephrinB ligands and EphB receptors in cardiovascular development: demarcation of arterial/venous domains, vascular morphogenesis, and sprouting angiogenesis. *Genes Dev.* **13,** 295–306 (1999).

4. Mohamed, A. M. & Chin-Sang, I. D. Characterization of loss-of-function and gain-of-function Eph receptor tyrosine kinase signaling in C. elegans axon targeting and cell migration. *Dev. Biol.* **290,** 164–76 (2006).

5. Miao, H. *et al.* Inhibition of integrin-mediated cell adhesion but not directional cell migration requires catalytic activity of EphB3 receptor tyrosine kinase. Role of Rho family small GTPases. *J. Biol. Chem.* **280,** 923–32 (2005).

6. Eph Nomenclature Committee. Unified nomenclature for Eph family receptors and their ligands, the ephrins. Eph Nomenclature Committee. *Cell* **90,** 403–4 (1997).

7. Lisabeth, E. M., Falivelli, G. & Pasquale, E. B. Eph receptor signaling and ephrins. *Cold Spring Harb. Perspect. Biol.* **5,** (2013).

8. Miao, H. & Wang, B. EphA receptor signaling--complexity and emerging themes. *Semin. Cell Dev. Biol.* **23,** 16–25 (2012).

9. Seiradake, E., Harlos, K., Sutton, G., Aricescu, A. R. & Jones, E. Y. An extracellular steric seeding mechanism for Eph-ephrin signaling platform assembly. *Nat. Publ. Gr.* **17,** 398–402 (2010).

10. Himanen, J. P. J. P. *et al.* Architecture of Eph receptor clusters. *Proc. Natl. Acad. Sci. U. S. A.* **107,** 10860–5 (2010).

11. Stapleton, D., Balan, I., Pawson, T. & Sicheri, F. The crystal structure of an Eph receptor SAM domain reveals a mechanism for modular dimerization. *Nat. Struct. Biol.* **6,** 44–9 (1999).

12. Wimmer-Kleikamp, S. H., Janes, P. W., Squire, A., Bastiaens, P. I. H. & Lackmann, M. Recruitment of Eph receptors into signaling clusters does not require ephrin contact. *J. Cell Biol.* **164,** 661–6 (2004).

13. Seiradake, E. *et al.* Structurally encoded intraclass differences in EphA clusters drive distinct cell responses. *Nat. Struct. Mol. Biol.* **20,** 958–64 (2013).

14. Miao, H. *et al.* EphA2 mediates ligand-dependent inhibition and ligand-independent promotion of cell migration and invasion via a reciprocal regulatory loop with Akt. *Cancer Cell* **16,** 9–20 (2009).

15. Miao, H. *et al.* EphA2 mediates ligand-dependent inhibition and ligand-independent promotion of cell migration and invasion via a reciprocal regulatory loop with Akt. *Cancer Cell* **16,** 9–20 (2009).

16. Wykosky, J. & Debinski, W. The EphA2 receptor and ephrinA1 ligand in solid tumors: function and therapeutic targeting. *Mol. cancer Res.* **6,** 1795–806 (2008).

17. Arvanitis, D. N. & Davy, A. Regulation and misregulation of Eph/ephrin expression. *Cell Adh. Migr.* **6,** 131–7 (2012).

18. Zelinski, D. P., Zantek, N. D., Stewart, J. C., Irizarry, A. R. & Kinch, M. S. EphA2 overexpression causes tumorigenesis of mammary epithelial cells. *Cancer Res.* **61,** 2301–6 (2001).

19. Ogawa, K. *et al.* The ephrin-A1 ligand and its receptor, EphA2, are expressed during tumor neovascularization. *Oncogene* **19,** 6043–52 (2000).

20. Macrae, M. *et al.* A conditional feedback loop regulates Ras activity through EphA2. *Cancer Cell* **8,** 111–8 (2005).

21. Vaught, D., Brantley-Sieders, D. M. & Chen, J. Eph receptors in breast cancer: roles in tumor promotion and tumor suppression. *Breast Cancer Res.* **10,** 217 (2008).

22. Pan, M. Overexpression of EphA2 gene in invasive human breast cancer and its association with hormone receptor status. *J. Clin. Oncol.* **23,** 9583 (2005).

23. Zhuang, G. *et al.* Elevation of receptor tyrosine kinase EphA2 mediates resistance to trastuzumab therapy. *Cancer Res.* **70,** 299–308 (2010).

24. Kaenel, P. The multifaceted roles of Eph-ephrin signaling in breast cancer. *Cell Adhes. …* **6,** 138–147 (2012).

25. Bissell, M. J. & Radisky, D. Putting tumours in context. *Nat. Rev. Cancer* **1,** 46–54 (2001).

26. Nelson, C. M., Vanduijn, M. M., Inman, J. L., Fletcher, D. A. & Bissell, M. J. Tissue geometry determines sites of mammary branching morphogenesis in organotypic cultures. *Science* **314,** 298–300 (2006).

27. Salaita, K. *et al.* Restriction of receptor movement alters cellular response: physical force sensing by EphA2. *Science* **327,** 1380–5 (2010).

28. Xu, Q., Lin, W. C. W.-C., Petit, R. S. R. S. & Groves, J. T. J. T. EphA2 receptor activation by monomeric Ephrin-A1 on supported membranes. *Biophys. J.* **101,** 2731–9 (2011).

29. Lohmüller, T., Xu, Q. & Groves, J. J. T. Nanoscale Obstacle Arrays Frustrate Transport of EphA2-Ephrin-A1 Clusters in Cancer Cell Lines. *Nano Lett.* **13,** 3059–3064 (2013).

30. Polo, S. & Di Fiore, P. P. Endocytosis conducts the cell signaling orchestra. *Cell* **124,** 897–900 (2006).

31. Liu, J., Sun, Y., Oster, G. F. & Drubin, D. G. Mechanochemical crosstalk during endocytic vesicle formation. *Curr. Opin. Cell Biol.* **22,** 36–43 (2010).

32. McMahon, H. T. H. T. & Boucrot, E. Molecular mechanism and physiological functions of clathrin-mediated endocytosis. *Nat. Rev. Mol. Cell Biol.* **12,** 517–33 (2011).

33. Sadowski, L., Pilecka, I., Miaczynska, M., Parachoniak, C. A. & Park, M. Dynamics of receptor trafficking in tumorigenicity. *Trends Cell Biol.* **22,** 231–40 (2012).

34. Wiley, H. S. & Burke, P. M. Regulation of receptor tyrosine kinase signaling by endocytic trafficking. *Traffic* **2,** 12–8 (2001).

35. Sadowski, L., Pilecka, I. & Miaczynska, M. Signaling from endosomes: location makes a difference. *Exp. Cell Res.* **315,** 1601–9 (2009).

36. Marston, D. J., Dickinson, S. & Nobes, C. D. Rac-dependent trans-endocytosis of ephrinBs regulates Eph-ephrin contact repulsion. *Nat. Cell Biol.* **5,** 879–88 (2003).

37. Zimmer, M., Palmer, A., Köhler, J. & Klein, R. EphB-ephrinB bi-directional endocytosis terminates adhesion allowing contact mediated repulsion. *Nat. Cell Biol.* **5,** 869–78 (2003).

38. Pitulescu, M. E. & Adams, R. H. Eph/ephrin molecules--a hub for signaling and endocytosis. *Genes Dev.* **24,** 2480–92 (2010).

39. Zhuang, G., Hunter, S., Hwang, Y. & Chen, J. Regulation of EphA2 receptor endocytosis by SHIP2 lipid phosphatase via phosphatidylinositol 3-Kinase-dependent Rac1 activation. *J. Biol. Chem.* **282,** 2683–94 (2007).

40. Irie, F., Okuno, M., Pasquale, E. B. & Yamaguchi, Y. EphrinB-EphB signalling regulates clathrin-mediated endocytosis through tyrosine phosphorylation of synaptojanin 1. *Nat. Cell Biol.* **7,** 501–9 (2005).

41. Wykosky, J. *et al.* Soluble monomeric EphrinA1 is released from tumor cells and is a functional ligand for the EphA2 receptor. *Oncogene* **27,** 7260–7273 (2008).

42. Beauchamp, A. *et al.* "EphrinA1 is released in Three Forms from Cancer Cells by Matrix Metalloproteases."*Mol. Cell. Biol.* **32,** (2012).

43. Lema Tomé, C. M. *et al.* Structural and functional characterization of monomeric EphrinA1 binding site to EphA2 receptor. *J. Biol. Chem.* **287,** 14012–22 (2012).

44. Groves, J. T. & Boxer, S. G. Electric field-induced concentration gradients in planar supported bilayers. *Biophys. J.* **69,** 1972–5 (1995).

45. Groves, J. T., Wülfing, C. & Boxer, S. G. Electrical manipulation of glycan-phosphatidyl inositol-tethered proteins in planar supported bilayers. *Biophys. J.* **71,** 2716–23 (1996).

46. Groves, J. T., Ulman, N. & Boxer, S. G. Micropatterning fluid lipid bilayers on solid supports. *Science* **275,** 651–3 (1997).

47. DeMond, A. L., Mossman, K. D., Starr, T., Dustin, M. L. & Groves, J. T. T cell receptor microcluster transport through molecular mazes reveals mechanism of translocation. *Biophys. J.* **94,** 3286–92 (2008).

48. Mossman, K. D. K. D., Campi, G., Groves, J. T. J. T. & Dustin, M. L. M. L. Altered TCR signaling from geometrically repatterned immunological synapses. *Science* **310,** 1191–3 (2005).

49. Janes, P. W. *et al.* Adam meets Eph: an ADAM substrate recognition module acts as a molecular switch for ephrin cleavage in trans. *Cell* **123,** 291–304 (2005).

50. Atapattu, L. *et al.* Antibodies binding the ADAM10 substrate recognition domain inhibit Eph function. *J. Cell Sci.* **125,** 6084–93 (2012).

51. Hattori, M., Osterfield, M. & Flanagan, J. G. Regulated Cleavage of a Contact-Mediated Axon Repellent. *Science (80-.).* **289,** 1360–1365 (2000).

52. Nye, J. a & Groves, J. T. Kinetic control of histidine-tagged protein surface density on supported lipid bilayers. *Langmuir* **24,** 4145–9 (2008).

53. Coyle, M. P., Xu, Q., Chiang, S., Francis, M. B. & Groves, J. T. DNA-mediated assembly of protein heterodimers on membrane surfaces. *J. Am. Chem. Soc.* **135,** 5012–6 (2013).

54. Lin, W. W.-C., Yu, C., Triffo, S. & Groves, J. T. Supported membrane formation, characterization, functionalization, and patterning for application in biological science and technology. *Curr. Protoc. Chem. Biol.* **2,** 235–69 (2010).

55. Seiradake, E., Harlos, K., Sutton, G., Aricescu, A. R. & Jones, E. Y. An extracellular steric seeding mechanism for Eph-ephrin signaling platform assembly. *Nat. Struct. Mol. Biol.* **17,** 398–402 (2010).

56. Berger, O., Edholm, O. & Jähnig, F. Molecular dynamics simulations of a fluid bilayer of dipalmitoylphosphatidylcholine at full hydration, constant pressure, and constant temperature. *Biophys. J.* **72,** 2002–13 (1997).

57. Domański, J., Stansfeld, P. J., Sansom, M. S. P. & Beckstein, O. Lipidbook: a public repository for force-field parameters used in membrane simulations. *J. Membr. Biol.* **236,** 255–8 (2010).

58. Lackmann, M. & Boyd, A. W. Eph, a protein family coming of age: more confusion, insight, or complexity? *Sci. Signal.* **1,** re2 (2008).

59. Adams, R. H. & Klein, R. Eph receptors and ephrin ligands. essential mediators of vascular development. *Trends Cardiovasc. Med.* **10,** 183–8 (2000).

60. Adams, R. H. *et al.* Roles of ephrinB ligands and EphB receptors in cardiovascular development: demarcation of arterial/venous domains, vascular morphogenesis, and sprouting angiogenesis. *Genes Dev.* **13,** 295–306 (1999).

61. Mohamed, A. M. & Chin-Sang, I. D. Characterization of loss-of-function and gain-of-function Eph receptor tyrosine kinase signaling in C. elegans axon targeting and cell migration. *Dev. Biol.* **290,** 164–76 (2006).

62. Miao, H. *et al.* Inhibition of integrin-mediated cell adhesion but not directional cell migration requires catalytic activity of EphB3 receptor tyrosine kinase. Role of Rho family small GTPases. *J. Biol. Chem.* **280,** 923–32 (2005).

63. Eph Nomenclature Committee. Unified nomenclature for Eph family receptors and their ligands, the ephrins. Eph Nomenclature Committee. *Cell* **90,** 403–4 (1997).

64. Wykosky, J. & Debinski, W. The EphA2 receptor and ephrinA1 ligand in solid tumors: function and therapeutic targeting. *Mol. cancer Res.* **6,** 1795–806 (2008).

65. Arvanitis, D. N. & Davy, A. Regulation and misregulation of Eph/ephrin expression. *Cell Adh. Migr.* **6,** 131–7 (2012).

66. Zelinski, D. P., Zantek, N. D., Stewart, J. C., Irizarry, A. R. & Kinch, M. S. EphA2 overexpression causes tumorigenesis of mammary epithelial cells. *Cancer Res.* **61,** 2301–6 (2001).

67. Ogawa, K. *et al.* The ephrin-A1 ligand and its receptor, EphA2, are expressed during tumor neovascularization. *Oncogene* **19,** 6043–52 (2000).

68. Macrae, M. *et al.* A conditional feedback loop regulates Ras activity through EphA2. *Cancer Cell* **8,** 111–8 (2005).

69. Vaught, D., Brantley-Sieders, D. M. & Chen, J. Eph receptors in breast cancer: roles in tumor promotion and tumor suppression. *Breast Cancer Res.* **10,** 217 (2008).

70. Pan, M. Overexpression of EphA2 gene in invasive human breast cancer and its association with hormone receptor status. *J. Clin. Oncol.* **23,** 9583 (2005).

71. Zhuang, G. *et al.* Elevation of receptor tyrosine kinase EphA2 mediates resistance to trastuzumab therapy. *Cancer Res.* **70,** 299–308 (2010).

72. Miao, H. *et al.* EphA2 mediates ligand-dependent inhibition and ligand-independent promotion of cell migration and invasion via a reciprocal regulatory loop with Akt. *Cancer Cell* **16,** 9–20 (2009).

73. Bissell, M. J. & Radisky, D. Putting tumours in context. *Nat. Rev. Cancer* **1,** 46–54 (2001).

74. Nelson, C. M., Vanduijn, M. M., Inman, J. L., Fletcher, D. A. & Bissell, M. J. Tissue geometry determines sites of mammary branching morphogenesis in organotypic cultures. *Science* **314,** 298–300 (2006).

75. Salaita, K. *et al.* Restriction of receptor movement alters cellular response: physical force sensing by EphA2. *Science* **327,** 1380–5 (2010).

76. Xu, Q., Lin, W.-C., Petit, R. S. & Groves, J. T. EphA2 receptor activation by monomeric Ephrin-A1 on supported membranes. *Biophys. J.* **101,** 2731–9 (2011).

77. Lohmüller, T., Xu, Q. & Groves, J. T. Nanoscale Obstacle Arrays Frustrate Transport of EphA2-Ephrin-A1 Clusters in Cancer Cell Lines. *Nano Lett.* **13,** 3059–3064 (2013).

78. Polo, S. & Di Fiore, P. P. Endocytosis conducts the cell signaling orchestra. *Cell* **124,** 897–900 (2006).

79. Liu, J., Sun, Y., Oster, G. F. & Drubin, D. G. Mechanochemical crosstalk during endocytic vesicle formation. *Curr. Opin. Cell Biol.* **22,** 36–43 (2010).

80. McMahon, H. T. & Boucrot, E. Molecular mechanism and physiological functions of clathrin-mediated endocytosis. *Nat. Rev. Mol. Cell Biol.* **12,** 517–33 (2011).

81. Parachoniak, C. A. & Park, M. Dynamics of receptor trafficking in tumorigenicity. *Trends Cell Biol.* **22,** 231–40 (2012).

82. Wiley, H. S. & Burke, P. M. Regulation of receptor tyrosine kinase signaling by endocytic trafficking. *Traffic* **2,** 12–8 (2001).

83. Marston, D. J., Dickinson, S. & Nobes, C. D. Rac-dependent trans-endocytosis of ephrinBs regulates Eph-ephrin contact repulsion. *Nat. Cell Biol.* **5,** 879–88 (2003).

84. Zimmer, M., Palmer, A., Köhler, J. & Klein, R. EphB-ephrinB bi-directional endocytosis terminates adhesion allowing contact mediated repulsion. *Nat. Cell Biol.* **5,** 869–78 (2003).

85. Pitulescu, M. E. & Adams, R. H. Eph/ephrin molecules--a hub for signaling and endocytosis. *Genes Dev.* **24,** 2480–92 (2010).

86. Zhuang, G., Hunter, S., Hwang, Y. & Chen, J. Regulation of EphA2 receptor endocytosis by SHIP2 lipid phosphatase via phosphatidylinositol 3-Kinase-dependent Rac1 activation. *J. Biol. Chem.* **282,** 2683–94 (2007).

87. Irie, F., Okuno, M., Pasquale, E. B. & Yamaguchi, Y. EphrinB-EphB signalling regulates clathrin-mediated endocytosis through tyrosine phosphorylation of synaptojanin 1. *Nat. Cell Biol.* **7,** 501–9 (2005).

88. Groves, J. T. & Boxer, S. G. Electric field-induced concentration gradients in planar supported bilayers. *Biophys. J.* **69,** 1972–5 (1995).

89. Groves, J. T., Wülfing, C. & Boxer, S. G. Electrical manipulation of glycan-phosphatidyl inositol-tethered proteins in planar supported bilayers. *Biophys. J.* **71,** 2716–23 (1996).

90. Wykosky, J., Palma, E., Gibo, D. & Ringler, S. Soluble monomeric EphrinA1 is released from tumor cells and is a functional ligand for the EphA2 receptor. *Oncogene* 7260–7273 (2008). doi:10.1038/onc.2008.328

91. Lema Tomé, C. M. *et al.* Structural and functional characterization of monomeric EphrinA1 binding site to EphA2 receptor. *J. Biol. Chem.* **287,** 14012–22 (2012).

92. Beauchamp, A. *et al.* "EphrinA1 is released in Three Forms from Cancer Cells by Matrix Metalloproteases."*Mol. Cell. Biol.* **32,** (2012).

93. Groves, J. T., Ulman, N. & Boxer, S. G. Micropatterning fluid lipid bilayers on solid supports. *Science* **275,** 651–3 (1997).

94. DeMond, A. L., Mossman, K. D., Starr, T., Dustin, M. L. & Groves, J. T. T cell receptor microcluster transport through molecular mazes reveals mechanism of translocation. *Biophys. J.* **94,** 3286–92 (2008).

95. Mossman, K. D., Campi, G., Groves, J. T. & Dustin, M. L. Altered TCR signaling from geometrically repatterned immunological synapses. *Science* **310,** 1191–3 (2005).

96. Doyon, J. B. *et al.* Rapid and efficient clathrin-mediated endocytosis revealed in genome-edited mammalian cells. *Nat. Cell Biol.* **13,** 331–7 (2011).

97. Triffo, S. B., Huang, H. H., Smith, A. W., Chou, E. T. & Groves, J. T. Monitoring lipid anchor organization in cell membranes by PIE-FCCS. *J. Am. Chem. Soc.* **134,** 10833–42 (2012).

98. Stauffer, T. P., Ahn, S. & Meyer, T. Receptor-induced transient reduction in plasma membrane PtdIns(4,5)P2 concentration monitored in living cells. *Curr. Biol.* **8,** 343–6 (1998).

99. Burkel, B. M., von Dassow, G. & Bement, W. M. Versatile fluorescent probes for actin filaments based on the actin-binding domain of utrophin. *Cell Motil. Cytoskeleton* **64,** 822–32 (2007).

100. Edelstein, A., Amodaj, N., Hoover, K., Vale, R. & Stuurman, N. Computer control of microscopes using μManager. *Curr. Protoc. Mol. Biol.* **92,** 14.20 (2010).

101. Schindelin, J. *et al.* Fiji: an open-source platform for biological-image analysis. *Nat. Methods* **9,** 676–82 (2012).

102. Bolte, S. & Cordelières, F. P. A guided tour into subcellular colocalization analysis in light microscopy. *J. Microsc.* **224,** 213–32 (2006).

103. Pettersen, E. F. *et al.* UCSF Chimera--a visualization system for exploratory research and analysis. *J. Comput. Chem.* **25,** 1605–12 (2004).

104. Fotin, A. *et al.* Molecular model for a complete clathrin lattice from electron cryomicroscopy. *Nature* **432,** 573–9 (2004).

105. Von Kleist, L. *et al.* Role of the clathrin terminal domain in regulating coated pit dynamics revealed by small molecule inhibition. *Cell* **146,** 471–84 (2011).

106. Dutta, D., Williamson, C. D., Cole, N. B. & Donaldson, J. G. Pitstop 2 is a potent inhibitor of clathrin-independent endocytosis. *PLoS One* **7,** e45799 (2012).

107. Fridman, J. S. *et al.* Selective inhibition of ADAM metalloproteases as a novel approach for modulating ErbB pathways in cancer. *Clin. Cancer Res.* **13,** 1892–902 (2007).

108. Zhou, B.-B. S. *et al.* Targeting ADAM-mediated ligand cleavage to inhibit HER3 and EGFR pathways in non-small cell lung cancer. *Cancer Cell* **10,** 39–50 (2006).

109. Le Roy, C. & Wrana, J. L. Clathrin- and non-clathrin-mediated endocytic regulation of cell signalling. *Nat. Rev. Mol. Cell Biol.* **6,** 112–26 (2005).

110. Heuser, J. & Kirchhausen, T. Deep-etch views of clathrin assemblies. *J. Ultrastruct. Res.* **92,** 1–27 (1985).

111. Boulant, S., Kural, C., Zeeh, J.-C., Ubelmann, F. & Kirchhausen, T. Actin dynamics counteract membrane tension during clathrin-mediated endocytosis. *Nat. Cell Biol.* **13,** 1124–31 (2011).

112. Stachowiak, J. C. *et al.* Membrane bending by protein-protein crowding. *Nat. Cell Biol.* **14,** 944–9 (2012).

113. Parthasarathy, R. & Groves, J. T. Curvature and spatial organization in biological membranes. *Soft Matter* **3,** 24 (2007).

114. Parthasarathy, R., Yu, C. & Groves, J. T. Curvature-modulated phase separation in lipid bilayer membranes. *Langmuir* **22,** 5095–9 (2006).

115. Rangamani, P., Agrawal, A., Mandadapu, K. K., Oster, G. & Steigmann, D. J. Interaction between surface shape and intra-surface viscous flow on lipid membranes. *Biomech. Model. Mechanobiol.* **12,** 833–45 (2013).

116. Sigismund, S. *et al.* Clathrin-mediated internalization is essential for sustained EGFR signaling but dispensable for degradation. *Dev. Cell* **15,** 209–19 (2008).

117. Carroll-Portillo, A. *et al.* Formation of a mast cell synapse: Fc epsilon RI membrane dynamics upon binding mobile or immobilized ligands on surfaces. *J. Immunol.* **184,** 1328–38 (2010).

118. Hartman, N. C., Nye, J. A. & Groves, J. T. Cluster size regulates protein sorting in the immunological synapse. *Proc. Natl. Acad. Sci. U. S. A.* **106,** 12729–34 (2009).

119. Xi, H.-Q., Wu, X.-S., Wei, B. & Chen, L. Eph receptors and ephrins as targets for cancer therapy. *J. Cell. Mol. Med.* **16,** 2894–909 (2012).

120. Kandouz, M. The Eph/Ephrin family in cancer metastasis: communication at the service of invasion. *Cancer Metastasis Rev.* **31,** 353–73 (2012).

121. Faoro, L. *et al.* EphA2 mutation in lung squamous cell carcinoma promotes increased cell survival, cell invasion, focal adhesions, and mammalian target of rapamycin activation. *J. Biol. Chem.* **285,** 18575–85 (2010).

122. Walker-Daniels, J., Riese, D. J. & Kinch, M. S. c-Cbl-dependent EphA2 protein degradation is induced by ligand binding. *Mol. Cancer Res.* **1,** 79–87 (2002).

123. Kinch, M. S. & Carles-Kinch, K. Overexpression and functional alterations of the EphA2 tyrosine kinase in cancer. *Clin. Exp. Metastasis* **20,** 59–68 (2003).

124. Dave, A., Laurie, K., Staffieri, S. & Taranath, D. Mutations in the EPHA2 Gene Are a Major Contributor to Inherited Cataracts in South-Eastern Australia. *PLoS One* **8,** e72518 (2013).

125. Shentu, X.-C., Zhao, S.-J., Zhang, L. & Miao, Q. A novel p.R890C mutation in EPHA2 gene associated with progressive childhood posterior cataract in a Chinese family. *Int. J. Ophthalmol.* **6,** 34–8 (2013).

126. Pasquale, E. B. Eph receptors and ephrins in cancer: bidirectional signalling and beyond. *Nat. Rev. Cancer* **10,** 165–80 (2010).

127. Lohmüller, T., Xu, Q. & Groves, J. Nanoscale Obstacle Arrays Frustrate Transport of EphA2–Ephrin-A1 Clusters in Cancer Cell Lines. *Nano Lett.* **13,** 3059–3064 (2013).

128. Annunziata, C. M. *et al.* Phase 1, open-label study of MEDI-547 in patients with relapsed or refractory solid tumors. *Invest. New Drugs* **31,** 77–84 (2013).

129. Jackson, D. *et al.* A human antibody-drug conjugate targeting EphA2 inhibits tumor growth in vivo. *Cancer Res.* **68,** 9367–74 (2008).

130. Ran, F. A. *et al.* Genome engineering using the CRISPR-Cas9 system. *Nat. Protoc.* **8,** 2281–308 (2013).

131. Greene, A. C. *et al.* Spatial organization of EphA2 at the cell-cell interface modulates trans-endocytosis of ephrinA1. *Biophys. J.* **106,** 2196–205 (2014).